HHS Public Access

Author manuscript

Nat Cancer. Author manuscript; available in PMC 2022 February 02.

Published in final edited form as:

Nat Cancer. 2021 September ; 2: 978–993. doi:10.1038/s43018-021-00237-1.

Autophagy Inhibition by Targeting PIKfyve Potentiates Response to Immune Checkpoint Blockade in Prostate Cancer

Yuanyuan Qiao[1,2,3], **Jae Eun Choi**[1,4], **Jean C. Tien**[1,2], **Stephanie A. Simko**[1], **Thekkelnaycke Rajendiran**[2,5], **Josh N. Vo**[1,6], **Andrew D. Delekta**[1], **Lisha Wang**[1], **Lanbo Xiao**[1], **Nathan B. Hodge**[1], **Parth Desai**[1], **Sergio Mendoza**[1], **Kristin Juckette**[1], **Alice Xu**[1], **Tanu Soni**[5], **Fengyun Su**[1], **Rui Wang**[1], **Xuhong Cao**[1,7], **Jiali Yu**[8], **Ilona Kryczek**[8], **Xiao-Ming Wang**[1,2], **Xiaoju Wang**[1], **Javed Siddiqui**[1], **Zhen Wang**[9], **Amélie Bernard**[10,11], **Ester Fernandez-Salas**[1], **Nora M. Navone**[12], **Stephanie J. Ellison**[1], **Ke Ding**[9], **Eeva-Liisa Eskelinen**[13], **Elisabeth I. Heath**[14], **Daniel J. Klionsky**[11], **Weiping Zou**[2,3,8], **Arul M. Chinnaiyan**[1,2,3,7,15,*]

[1]Michigan Center for Translational Pathology, University of Michigan, Ann Arbor, Michigan 48109, USA.

[2]Department of Pathology, University of Michigan, Ann Arbor, Michigan 48109, USA.

[3]Rogel Cancer Center, University of Michigan, Ann Arbor, Michigan 48109, USA.

[4]School of Medicine, University of California, San Diego, California 92093, USA.

[5]Michigan Regional Comprehensive Metabolomics Resource Core, Ann Arbor, Michigan 48109, USA.

[6]Department of Computational Medicine and Bioinformatics, University of Michigan, Ann Arbor, Michigan 48109, USA.

[7]Howard Hughes Medical Institute, University of Michigan, Ann Arbor, Michigan 48109, USA.

[8]Department of Surgery, University of Michigan Medical School, Ann Arbor, Michigan 48109, USA.

[*]Correspondence to: Arul M. Chinnaiyan, Michigan Center for Translational Pathology, Rogel Cancer Center, 1500 East Medical Center Drive, Ann Arbor, Michigan 48109, USA. Phone: 734-615-4062; Fax: 734-615-4498; arul@umich.edu.

AUTHOR CONTRIBUTIONS

Y.Q. and A.M.C. participated in the planning, initiation, and overall analysis of data as well as writing, reviewing, and editing of the manuscript. Y.Q., S.A.S., A.D.D., N.B.H., P.D., and S.M. performed *in vitro* and *in vivo* experiments. J.C.T., J.E.C., K.J., and A.X. participated in *in vivo* experiments. Y.Q., T.R., and T.S. participated in lipidomics experimental design and data analysis. Z.W. and K.D. participated in the execution of chemical synthesis of ESK981. L.W., X.-M.W., and J.S. performed histological sample preparation, staining, and interpretation of RNA-ISH results. L.X. helped with CRISPR *Atg5* knockout design. X.W. assisted with ELISA experiments. X.C., F.S., R.W., and J.N.V. performed RNA-seq library preparation, sequencing, and data analysis. J.Y., I. K., and J.E.C. participated in flow cytometry analysis. A.B. and D.J.K. participated in yeast experiments and data interpretation. E.L.E. performed electron microscopy analysis, and E.L.E. and D.J.K. participated in autophagy data interpretation. N.M.N. provided patient-derived xenograft models. S.J.E. participated in writing and preparation of this manuscript. W.Z. participated in immune checkpoint blockade experimental design and data interpretation. E.F.S., E.I.H., and A.M.C. provided project oversight for clinical trial design and review based on the interpretation of this preclinical data.

COMPETING INTERESTS

The University of Michigan has filed a disclosure on the findings based on this study. A.M.C. and Y.Q. are named as co-inventors on the disclosure. Esanik Therapeutics, Inc. licensed ESK981 from Teva Pharmaceuticals. A.M.C. is a co-founder and serves on the scientific advisory board of Esanik Therapeutics, Inc. Esanik Therapeutics or Teva Pharmaceuticals were not involved in the design or approval of this study, nor was this study funded by them. The remaining authors declare no competing interests.

[9]School of Pharmacy, Jinan University, Guangzhou 510632, China.

[10]CNRS, Laboratoire de Biogenèse Membranaire, UMR5200; Université de Bordeaux, Laboratoire de Biogenèse Membranaire, UMR5200, 33000 Bordeaux, France.

[11]Life Sciences Institute and Department of Molecular, Cellular and Developmental Biology, University of Michigan, Ann Arbor, Michigan 48109, USA.

[12]Department of Genitourinary Medical Oncology, The University of Texas MD Anderson Cancer Center, Houston, Texas 77030, USA.

[13]Institute of Biomedicine, University of Turku, 20520 Turku, Finland.

[14]Karmanos Cancer Institute, Department of Oncology, Wayne State University School of Medicine, Detroit, Michigan 48201, USA.

[15]Department of Urology, University of Michigan, Ann Arbor, Michigan 48109, USA.

Abstract

Multi-tyrosine kinase inhibitors (MTKIs) have thus far had limited success in the treatment of castration-resistant prostate cancer (CRPC). Here, we report a phase I-cleared orally bioavailable MTKI, ESK981, with a novel autophagy inhibitory property that decreased tumor growth in diverse preclinical models of CRPC. The anti-tumor activity of ESK981 was maximized in immunocompetent tumor environments where it upregulated *CXCL10* expression through the interferon gamma pathway and promoted functional T cell infiltration, which resulted in enhanced therapeutic response to immune checkpoint blockade. Mechanistically, we identify the lipid kinase PIKfyve as the direct target of ESK981. PIKfyve-knockdown recapitulated ESK981's anti-tumor activity and enhanced the therapeutic benefit of immune checkpoint blockade. Our study reveals that targeting PIKfyve via ESK981 turns tumors from cold into hot through inhibition of autophagy, which may prime the tumor immune microenvironment in advanced prostate cancer patients and be an effective treatment strategy alone or in combination with immunotherapies.

INTRODUCTION

Although advanced prostate cancer often initially responds to therapies that suppress androgen signaling, resistance inevitably develops, leading to the emergence of castration-resistant prostate cancer (CRPC)[1]. Several developments in the past decade have advanced CRPC treatment, including enzalutamide and abiraterone, agents that target continued androgen receptor (AR) signaling[2,3]; however, these and other therapies for CRPC are not curative. In response to the hypothesis that combination treatments may be required to achieve durable responses in advanced cancers[4,5], the utility of multi-tyrosine kinase inhibitors (MTKIs) has been explored. Despite promising phase II clinical trial results with the MTKI cabozantinib in CRPC[6], the phase III trial failed to meet its primary survival endpoint[7]. In this study, we determined whether alternative phase I-cleared MTKIs could be repositioned for the treatment of advanced prostate cancer and have identified ESK981 as an effective monotherapy with an autophagy inhibitory property that also potentiates immunotherapeutic responses.

ESK981 (formerly CEP-11981) is an oral MTKI originally developed as an angiogenesis inhibitor targeting key kinases implicated in angiogenesis (FLT1/VEGFR-1, KDR/VEGFR-2, TEK/Tie-2)[8]. Importantly, ESK981 cleared a phase I dose-escalation study in patients with advanced, relapsed, or refractory solid tumors where the maximum-tolerated dose was 97.4 mg/m^2 daily[9]. Of the evaluable patients, 51% achieved stable disease at ≥6 weeks of ESK981 treatment. Serendipitously, our current study uncovers a novel mechanism of action of ESK981 that involves robust inhibition of autophagy through direct targeting of PIKfyve, a class III lipid kinase that converts phosphatidylinositol 3-phosphate (PI(3)P) to phosphatidylinositol 3,5-bisphosphate (PI(3,5)P_2)[10]. Studies of PIKfyve as a therapeutic target have thus far been limited to non-Hodgkin lymphoma, multiple myeloma, and non-small cell lung cancer[11-13].

The role of autophagy has been intensely studied in cancer[14], and several reports have suggested that autophagy inhibition may sensitize tumors to immune checkpoint inhibitors through release of T cell-attracting chemokines[15-17] or other immunomodulatory mechanisms[18]. In this study, we demonstrate that inhibition of autophagic flux, triggered by ESK981 or PIKfyve inhibition, renders prostate tumors toward an immune-responsive state, conferring sensitivity to immunotherapy. These findings have important implications for those cancers, such as prostate, that are not intrinsically immunogenic and have had limited success with immunotherapy[19,20].

RESULTS

Efficacy of ESK981 in advanced prostate cancer models

To determine whether MTKIs have the potential to be repositioned for CRPC, a cell viability screen employing a 167-compound library was performed in DU145 prostate cancer cells (Fig. 1a). From this screen, ESK981 was identified as a top candidate MTKI that decreased cell viability. ESK981 exhibited potent growth inhibition at 300 nM, an effect comparable to SRC inhibitors (KX2-391, dasatinib)[21] and the ERBB2/HER2 inhibitor mubritinib[22], compounds previously reported to target DU145 cells. Conversely, crizotinib and cabozantinib, MTKIs that have been evaluated clinically in CRPC[6,7,23,24], exhibited no growth inhibitory effects at the equivalent concentration (Fig. 1a). ESK981 was also found to trigger a cytoplasmic vacuolization morphology that was not observed with the other 167 compounds, including crizotinib and cabozantinib (Fig. 1b). Given that the top known targets of ESK981, VEGFR-1 and VEGFR-2, are not endogenously expressed in prostate cancer cells, this suggested that ESK981 had another uncharacterized mechanism of action in this setting.

The viability of diverse prostate cancer cell lines in response to ESK981 was therefore analyzed in long-term survival assays. ESK981 exhibited growth inhibitory IC_{50} values ranging from 37 to 207 nM across cell lines, including AR-positive (VCaP, LNCaP, 22RV1, C4-2B, LNCaP-AR) and AR-negative (PC3, DU145). In contrast, cabozantinib and crizotinib exhibited micromolar IC_{50} values (Fig. 1c, Extended Data Fig. 1a-b). In two enzalutamide-resistant cell lines, LNCaP-AR and CWR-R1, ESK981 remained efficacious (Fig. 1d). ESK981 sensitivity was further tested using a 3D-spheroid culture

system[25,26], and ESK981 produced a more robust inhibitory effect at lower concentrations than cabozantinib in VCaP 3D-spheroid culture (Fig. 1e).

The effect of ESK981 on other cellular functions was also assessed. Cell cycle analysis indicated that ESK981 induced a dose-dependent G_2/M-phase arrest in all prostate cancer cell lines tested (Extended Data Fig. 1c-d). In comparison with other inhibitors in VCaP cells (cabozantinib, crizotinib, enzalutamide), ESK981 demonstrated greater G_2/M arrest potential at a lower concentration. Additionally, ESK981 inhibited invasion in a dose-dependent manner in prostate cancer cells (Extended Data Fig. 1e).

To determine whether ESK981-mediated growth inhibition *in vitro* translated into anti-tumor effects, the efficacy of ESK981 in mouse xenograft models of prostate cancer was assessed. VCaP cells were chosen for initial experiments as they harbor the *TMPRSS2:ERG* gene fusion and *AR* amplification, frequent molecular aberrations in patients with advanced CRPC[27]. A castration-resistant VCaP tumor-bearing xenograft mouse model was generated to mimic clinical disease progression (Extended Data Fig. 2a). A previous study indicated that ESK981 treatment at 30 mg/kg twice daily for 28 consecutive days was well-tolerated with no apparent toxicity in tumor-bearing mice[8]. Thus, we started ESK981 at a regimen of 30 mg/kg or 60 mg/kg once daily for five days on/two days off for four weeks. ESK981 treatment resulted in significant dose-dependent growth inhibiton of castration-resistant VCaP xenografts, as well as reductions in tumor weight (Fig. 2a) and cell proliferation, assessed by MKI67/Ki67 immunohistochemistry (IHC) (Extended Data Fig. 2b). While minor temporary body weight losses were observed in the ESK981 60 mg/kg group following dosing, the body weights of 30 mg/kg ESK981-treated mice were not affected (Fig. 2a).

The efficacy of 30 mg/kg ESK981 was thus assessed in three additional prostate cancer xenograft models: MDA-PCa-146-12, an AR-positive patient-derived xenograft (PDX); DU145, an AR-negative prostate cancer cell line; and MDA-PCa-146-10, an AR-negative and neuroendocrine prostate cancer PDX. Significant inhibition of tumor growth by ESK981 was observed in all three models (Fig. 2b-d), and this was mirrored by significant decreases in tumor weights and Ki67 IHC (Extended Data Fig. 2c-d). Across the three models, no significant body weight loss was observed (Fig. 2b-d). Additionally, hematoxylin and eosin (H&E) staining showed that the dose-dependent vacuolization phenomenon was recapitulated *in vivo* in ESK981-treated VCaP tumors (Fig. 2e). Importantly, even at a 50 mg/kg dose of ESK981 five days per week, no abnormalities in major organ function or histology of various viceral organs were observed (Extended Data Fig. 3a-e). No organs were found to have the same tissue vacuolization morphology observed in tumors (Extended Data Fig. 3e-f). ESK981 is, therefore, well-tolerated *in vivo* and possesses broad anti-tumor potential for major subtypes of advanced prostate cancer, while also triggering a tumor-specific vacuolization morphology.

ESK981 inhibits autophagic flux in prostate cancer cells

Autophagy is an evolutionarily conserved, orderly process of degradation and destruction of cellular components. As part of this process, double-membraned vesicles called autophagosomes are formed following the engulfment of cytoplasmic constituents;

autophagosomes then fuse with lysosomes to form autolysosomes and initiate degradation and recycling of cargo[28]. The nature of the ESK981-associated cellular vacuolization was investigated in combination with autophagic pathway inhibitors. The early autophagosome inhibitor 3-methyladenine (3-MA) partially negated the vacuolization effects of ESK981 in DU145 cells (Fig. 3a). The anti-malarial drug chloroquine (CQ) and the vacuolar-type H^+-ATPase inhibitor bafilomycin A_1 (BF), inhibitors of autophagy and lysosomal fusion[29], completely blocked the vacuolization effects of ESK981 (Fig. 3a), suggesting that these vacuoles were linked to autophagic processes.

To measure the ability of ESK981 to impact autophagosome content, we employed the CYTO-ID® assay, which measures autophagosomes with minimal lysosomal staining[30]. Data showed dose-dependent inductions of autophagosomes by ESK981 in LNCaP, VCaP (Fig. 3b), and DU145 cells (Extended Data Fig. 4a). Levels of autophagosome induction by ESK981 (300 nM) were higher than the mTOR inhibitor rapamycin (10 μM), a well-known autophagy activator (Fig. 3b). Analysis of ESK981 and two compound libraries (154 autophagy-related compounds and 167 TKIs) at equivalent concentrations found that ESK981 was the top inducer of autophagosomes (Fig. 3c). The other top candidates were mTOR inhibitors and well-known kinase inhibitors reported to possess autophagosome induction capability. As a further measure of autophagosome levels, the state of MAP1LC3A/B (LC3) was assessed[29]. During autophagy, the cytosolic form of LC3 (LC3-I) gets recruited to the phagophore (the autophagosome precursor) membrane where it is conjugated to phosphatidylethanolamine (PE) to generate the lipidated form, LC3-II. Numerous prostate cancer cell lines were tested and exhibited an increase in the total level of LC3 lipidation in an ESK981 dose-dependent manner (Fig. 3d). Increased LC3-II levels were seen within three hours of 300 nM ESK981 treatment (Extended Data Fig. 4b). In contrast, cabozantinib did not induce LC3-II, even after 1 μM treatment for 24 hours. Likewise, crizotinib did not increase LC3-II levels at 300 nM and only weakly induced LC3-II at 1 μM (Extended Data Fig. 4c).

Much of our fundamental understanding of the autophagic process comes from seminal work in yeast[31]. To determine whether ESK981 impinged upon a conserved autophagic process, we utilized a drug-sensitive yeast strain (*pdr5Δ*) and analyzed Atg8, the yeast homolog to LC3. ESK981 treatment resulted in increased lipidated Atg8 levels (Extended Data Fig. 4d) similar to the results observed in prostate cancer cells with LC3, indicating ESK981 has a common target in yeast. However, eukaryotic-like tyrosine kinases are absent in yeast[32], which suggested that ESK981-induced autophagosome levels were independent of tyrosine kinase inhibition and likely involved targeting of a different kinase class.

To further analyze autophagosome levels in prostate cancer cells, GFP-LC3 puncta formation was monitored after various ESK981 treatment durations. ESK981 induced LC3 puncta formation in DU145 cells within one hour (Fig. 3e), prior to ESK981-induced vacuole formation, which was only observed after four hours. To better visualize subcellular components, transmission electron microscopy (TEM) was performed on DU145 cells and demonstrated mostly clear vacuoles adjacent to double-membraned autophagic vesicles after 24 hours of ESK981 (Fig. 4a). Vacuoles containing cellular materials were also observed by TEM of ESK981-treated tumors (Fig. 4b). Collectively, these results suggested

that the large empty vacuoles induced by ESK981 were unlikely to be autophagosomes. Indeed, immunofluorescence showed that ESK981-induced vacuoles stained positive for the lysosomal marker LAMP1 (Fig. 4c). LysoTracker Green assays confirmed that ESK981 increased lysosome quantity, and this response was neutralized by the vacuolar-type H+-ATPase inhibitor BF (Fig. 4d).

Autophagy is a dynamic process, and increased autophagosome and lysosome levels could be due to either activation or inhibition of autophagic flux. To measure autophagic flux, we utilized a GFP-LC3-RFP-LC3ΔG probe developed by Mizushima and colleagues[33]. This probe allows for direct assessment of autophagic flux without being combined with lysosomal inhibitors. When expressed in cells, the GFP-LC3-RFP-LC3ΔG probe is cleaved into a degradable fragment, GFP-LC3, and a stable fragment, RFP-LC3ΔG. A decrease of the GFP/RFP ratio indicates the occurrence of high autophagic flux. In GFP-LC3-RFP-LC3ΔG-expressing PC3 or DU145 cells, the mTORC inhibitor Torin1 decreased the GFP/RFP ratio, suggesting high autophagic flux (Fig. 4e). Conversely, ESK981, CQ, and BF all showed low autophagic flux (Fig. 4e). These results indicate that increased autophagosome and lysosome signals are likely due to decreased autophagic flux with ESK981 treatment.

To further determine the essential regulators of ESK981-induced autophagosome and lysosome accumulation, several autophagic pathway regulators were investigated. ULK1, Beclin1, FIP200, ATG5, and ATG7 were targeted with siRNA in LNCaP and VCaP cells, and only ATG5 or ATG7 inhibition demonstrated consistent blockage or reduction of ESK981- or sunitinib-induced LC3 lipidation (Extended Data Fig. 4e). The association between ESK981-induced effects and autophagy was further validated by genetic targeting of *Atg5*[28]. Vacuolization was significantly induced by ESK981 in wild-type mouse embryonic fibroblasts (MEFs) but attenuated in autophagy-deficient *Atg5*−/− MEFs (Fig. 4f). As expected, ESK981-induced LC3 lipidation was abolished in *Atg5* knockout MEFs (Fig. 4f). These results propose that ESK981-induced autophagosome and lysosome accumulations, associated with a vacuolization morphology, are ATG5-dependent and result from autophagic flux inhibition.

ESK981 increases CXCL10 and potentiates anti-PD-1 responses

Autophagy inhibition has been linked with cellular secretory processes, including release of cytokines into the tumor microenvironment[15,17,34,35]. Accordingly, in a human cytokine array, ESK981 significantly induced CXCL10 and, to a lesser extent, CCL2 in VCaP-conditioned media (Fig. 5a). Comparing ESK981 to the TKI and autophagy-linked compound libraries, ESK981 was the top inducer of CXCL10, as analyzed by ELISA (Fig. 5b). Well-known autophagy regulators rapamycin and Torin1 only marginally increased CXCL10 secretion (Extended Data Fig. 5a). *CXCL10* expression is physiologically regulated by interferon gamma (IFNγ)[36]. In multiple human prostate cancer cell lines, ESK981 enhanced expression of *CXCL10* in the presence of IFNγ (Extended Data Fig. 5b), suggesting that the ESK981-mediated autophagic process may play a role in immune response.

CXCL10 has been implicated in T cell recruitment in melanoma[37], implying that ESK981 may exert an immune response in prostate cancer through upregulation and secretion of this chemokine[38,39]. To investigate this premise, a mouse syngeneic prostate cancer model driven by human MYC expression (Myc-CaP)[40,41] was used. In Myc-CaP cells, ESK981 had a growth inhibitory IC_{50} value of 35 nM, compared to 2.3 μM for crizotinib and 263 nM for cabozantinib (Extended Data Fig. 5c). Accumulation of autophagosomes by ESK981 was recapitulated in Myc-CaP cells (Extended Data Fig. 5d), and autophagic flux was inhibited in GFP-LC3-RFP-LC3ΔG-expressing Myc-CaP cells after ESK981, CQ, or BF treatment (Extended Data Fig. 5e). We further generated *Atg5* knockout Myc-CaP cells, and consistent with the data in human prostate cancer cell lines, *Atg5* knockout in Myc-CaP cells significantly blocked ESK981-induced LC3 lipidation (Extended Data Fig. 6a). The lysosome vacuolization morphology and autophagosome levels were also decreased compared to parental cells (Extended Data Fig. 6b-c). Similar to human prostate cancer cell lines, ESK981 was able to enhance IFNγ regulation of CXCL10 secretion and expression (and *Cxcl9*) in Myc-CaP cells (Extended Data Fig. 6d-f). However, this phenomenon was diminished in *Atg5* knockout cells, further suggesting that CXCL10 levels are directly impacted by the autophagy pathway. Combined, these data indicate that the mechanism of action of ESK981 is consistent between human and mouse prostate cancer models.

Myc-CaP tumors were next established in immunocompetent FVB mice and treated with vehicle or ESK981 (15 mg/kg, 30 mg/kg). Tumor burden, visualized by bioluminescence intensity, indicated that five out of ten tumors were bioluminescent-negative in the 30 mg/kg group (Fig. 5c). ESK981-treated tumors demonstrated dose-dependent growth inhibition and significantly increased doubling time (Fig. 5d). In addition, analysis of mRNA levels of the T cell marker *Cd3* showed a dose-dependent upregulation in ESK981-treated tumors, as did *Cxcl10* (Fig. 5e). Flow cytometry demonstrated a significant increase in the infiltration of immune effector $CD8^+$ T cells, $CD4^+$ T cells, and total $CD3^+$ T cells in both $CD45^+$ lymphocytes and Myc-CaP tumors after ESK981 treatment (Fig. 5f). The ESK981-induced tumor-infiltrating $CD8^+$ and $CD4^+$ T cells produced higher levels of IFNγ and tumor necrosis factor α (TNFα) (Fig. 5g), indicating ESK981 both increases T cell infiltration and enhances activation. Additionally, the growth inhibitory effect mediated by ESK981 was examined by blocking the CXCL10 pathway or T cells. Myc-CaP tumor proliferation was partially negated by neutralizing anti-CXCR3 (the receptor for CXCL10 and CXCL9) antibody (Fig. 5h). Of note, combined $CD4^+$ and $CD8^+$ T cell depletion in ESK981-treated Myc-CaP tumors significantly, but not completely, increased tumor volume, suggesting that ESK981's anti-tumor effect is largely dependent on T cells (Fig. 5i). Since ESK981 also exerts anti-tumor effects in human prostate cancer xenografts in immune-deficient mice (Fig. 2a-d), these combined data suggest that ESK981's anti-tumor effect is maximized in the immunocompetent tumor environment through enhanced infiltration and activation of T cells.

These results prompted us to examine whether ESK981 was able to modulate the efficacy of checkpoint blockade immunotherapy. Tumors were established and treated with vehicle, 15 mg/kg ESK981, anti-PD-1 (Pdcd1), or a combination of ESK981 and anti-PD-1 (Fig. 6a). Anti-PD-1 demonstrated a tumor inhibitory effect that was strongly enhanced by ESK981 co-treatment (Fig. 6b); the slight increase in average tumor volume near

day 30 in the combination group was due to one outlier tumor that grew and reached endpoint. Individual tumor weight was markedly decreased in the ESK981 and anti-PD-1 combination group compared with ESK981 monotherapy (Fig. 6b). Combination ESK981 and anti-PD-1 treatment was well-tolerated and had no adverse impact on body weights of tumor-bearing mice (Fig. 6c). ESK981-treated groups showed elevated LC3 lipidation, confirming autophagosome accumulation in tumors (Fig. 6d). Consistently, *Cd3* mRNA levels were upregulated in both the ESK981 solo and combination treatment groups (Fig. 6e). The increased infiltration of $CD3^+$ T cells into Myc-CaP tumors was confirmed by *Cd3e* RNA *in situ* hybridization (ISH), with anti-PD-1 and ESK981 each increasing $CD3^+$ T cell trafficking in the tumor microenvironment and combination treatment having the largest increase over vehicle (Fig. 6e); a similar effect was observed for *Cxcl10* RNA ISH (Fig. 6f). Immune activation was further confirmed by transcriptomic analysis from individual tumors, which showed upregulation of inflammatory responses and *Cxcl10* with combination treatment (Extended Data Fig. 7).

Several murine syngeneic cancer cell lines in addition to those from the prostate lineage were analyzed in viability assays (Extended Data Fig. 8a). ESK981 treatment resulted in significant increases in autophagosome levels in murine cancer cell lines originating from different tissue types that included lung, melanoma, ovarian, pancreas, kidney, and breast (Extended Data Fig. 8b). Increased *Cxcl10* expression in the presence of mouse IFNγ was significantly enhanced by ESK981 in most cell lines tested (Extended Data Fig. 8c). In the 4T1 breast cancer model, which is resistant to immune checkpoint inhibitors, we demonstrated that ESK981 sensitized tumor cells to anti-PD-1, resulting in significant reduction in tumor burden and increased survival rates with combination ESK981 and anti-PD-1 treatment (Extended Data Fig. 9). Taken together, these results suggest that ESK981 increases CXCL10 secretion by blocking autophagic flux in tumor cells, resulting in T cell recruitment to the tumor microenvironment and enhanced therapeutic benefit of anti-PD-1 therapy in prostate and other cancers.

ESK981 directly targets PIKfyve to inhibit autophagy

Interestingly, RNA-seq analysis of ESK981-treated VCaP cells found that several genes regulated by ESK981 belonged to lipid, cholesterol, and steroid metabolic processes (Fig. 7a), indicating that ESK981 plays a role in cellular lipid production. Untargeted lipidomic analysis demonstrated that phosphatidylethanolamine (PE) was one of the major lipids increased by ESK981 (Fig. 7b). As mentioned above, PE is an important membrane component for phagophores, autophagosomes, and autolysosomes, and increased intracellular PE levels can positively regulate autophagosome biogenesis[42]. These results suggested that ESK981 directly targeted a factor involved in cellular lipid metabolism to impact autophagy.

To test whether ESK981 inhibited a lipid kinase, we performed an affinity binding screen for 22 phosphoinositide kinases and found ESK981 exhibited 100% inhibition for the lipid kinase PIKfyve (Fig. 7c). The dissociation constant (Kd) for ESK981 against PIKfyve was 12 nM, while those for PIP5K1C, PIP5K1A, and PIK3CA were 210 nM, 230 nM, and >10 μM, respectively (Fig. 7d). PIKfyve has been reported to maintain lysosome homeostasis;

direct inhibition of PIKfyve in mammalian cells, or the yeast homolog Fab1, resulted in a vacuolization morphology and decreased autophagic flux[11,43-45]. In order to determine whether PIKfyve was responsible for ESK981-associated vacuolization, individual lipid kinases were targeted, and only *PIKFYVE* knockdown generated a vacuolization phenotype resembling ESK981 treatment (Fig. 7e, Extended Data Fig. 10a-b). Autophagosome levels increased after *PIKFYVE* knockdown to levels similar to those induced by ESK981 in prostate cancer cells (Fig. 7f-g). Accumulation of autophagosome content and vacuolization morphology after *Pikfyve* knockdown were confirmed in additional types of murine cancer cell lines (Extended Data Fig. 10c-d). The cellular target engagement of ESK981 on PIKfyve was confirmed by a cellular thermal shift assay in VCaP cells, with the known PIKfyve inhibitor apilimod serving as a positive control (Fig. 7h). We further confirmed that knockdown of *PIKFYVE* increased *CXCL10* expression and enhanced IFNγ-mediated responses in human prostate cancer cells (Fig. 7i). We, therefore, identify PIKfyve as a direct target of ESK981 that affects cellular lipid metabolism and autophagic flux, thereby increasing *CXCL10* expression.

Pikfyve genetic inhibition enhances anti-PD-1 responses

To investigate whether PIKfyve inhibition is reponsible for the anti-tumor effects and immune responses mediated by ESK981, doxycycline-inducible *Pikfyve* knockdown (sh*Pikfyve*) Myc-CaP cells were generated. Upon *Pikfyve* knockdown, Myc-CaP cells displayed a vacuolization morphology resembling ESK981 treatment (Fig. 8a). Tumor proliferation was measured with sh*Pikfyve* Myc-CaP cells in both immune-competent (FVB) and immune-deficient (NSG) mice (Fig. 8b). Tumor proliferation and waterfall plots of individual mice showed that *Pikfyve* knockdown had greater tumor inhibitory effects in FVB than NSG mice (Fig. 8c-d). Similar to ESK981, these results suggest that PIKfyve inhibition can impact tumor growth in immunodeficient settings, but a competent immune environment can maximize its anti-tumor properties.

Finally, the effects of *Pikfyve* knockdown in combination with anti-PD-1 were examined using the Myc-CaP model (Fig. 8e). Similar to ESK981, *Pikfyve* knockdown resulted in significant tumor inhibition in FVB mice, and combination treatment with anti-PD-1 further enhanced the effect (Fig. 8f). Combination anti-PD-1 and *Pikfyve* knockdown significantly increased complete tumor regression, defined as the percent cure rate, of Myc-CaP tumors from 0 to 40% (Fig. 8f).

DISCUSSION

This study identifies ESK981 as an effective anti-tumor agent in multiple models of advanced prostate cancer and establishes PIKfyve as a novel target of ESK981. PIKfyve inhibition blocks autophagic flux, leading to increased CXCL10 expression and recruitment of T cells into the tumor microenvironment. PIKfyve inhibition ultimately converts prostate cancers from immune-cold to immune-hot, thereby increasing their susceptibility to immune checkpoint blockade (Fig. 8g). As a MTKI, ESK981 could potentially target PIKfyve in tumor cells as well as other known kinase targets (e.g., VEGF receptors)[8] in the tumor microenvironment important for neo-angiogenesis, thus inhibiting multiple essential targets

with one compound. Since anti-angiogenic agents were also reported to be effective in enhancing immune checkpoint inhibitor response[46], we used genetic inhibition to verify that direct targeting of *Pikfyve* itself is sufficient to block prostate cancer proliferation and enhance anti-PD-1 therapy. Whether PIKfyve plays a role in tumor angiogenesis is not known.

Molecular analysis uncovered the interesting finding that ESK981-induced autophagosome accumulation was recapitulated in yeast, even though eukaryotic-like tyrosine kinases are absent[32]. A subsequent kinase screen led to the discovery of the lipid kinase PIKfyve as the mediator of ESK981-induced cellular vacuolization and inhibition of authophagic flux. These findings are consistent with results obtained from inhibition or genetic inactivation of PIKfyve in mammalian cells, or the orthologue Fab1 in yeast [43,47-49]. Genetic inactivation of *Pikfyve* in Myc-CaP cells in our study excluded the potential contributions of other known targets of ESK981 in mediating autophagy inhibition in prostate cancer. Although previous studies have analyzed the anti-tumor effects of PIKfyve inhibition, such as in B cell non-Hodgkin's lymphoma[11], our study is the first to demonstrate that PIKfyve is a therapeutic target in advanced prostate cancer.

Autophagy inhibition has been intensely studied and shown to prevent tumor progression in multiple cancer types[34,50-52]. For example, in a genetically engineered mouse model, prostate-specific deletion of *Atg7* decreased *Pten*-deficient prostate tumor progression[53]. Autophagy has also been shown to be a treatment resistance and survival mechanism, including mediating enzalutamide resistance in CRPC[50]. As supported by our data, studies have emerged detailing the interplay between autophagy inhibition and anti-tumor immune responses[15-18]. As a recent example, tumor-intrinsic autophagy inhibition by VPS34-targeting recruits T and NK cells into the tumor microenvironment through increased expression of CXCL10 and CCL5 in multiple syngeneic murine models, resulting in enhanced therapeutic benefit of anti-PD-1/PD-L1[15]. Moreover, host autophagy can support tumor growth; systemic deletion of *Atg7* in mice significantly reduced the growth of melanoma models through degradation of arginine[34]. Host deletion of *Atg7* also increased circulating proinflammatory cytokine levels, including CXCL10, and promoted T cell infiltration in tumors with high mutational burden[54].

Prostate cancers are poorly immune-infiltrated, and immune checkpoint inhibitor monotherapy in unselected advanced prostate cancer patient populations has had minimal success. In phase III trials, the CTLA4 inhibitor ipilimumab failed to improve overall survival, while the PD-1 inhibitor pembrolizumab had low response rates (3-5%) in metastatic CRPC (mCRPC) patients[19,20,55]. In the 5-10% of advanced prostate cancers harboring mismatch repair deficiency/microsatellite instability and the 5-7% of patients harboring *CDK12* loss-of-function mutations, upregulated mutation-associated neoantigens render these tumors more susceptible to immunotherapy, yet only 50% response rates are achieved[56-59]. Thus, overcoming resistance to immune checkpoint blockade-based therapies and increasing their objective response rates remains an important challenge. Our study establishes the first proof-of-concept to design clinical trials using PIKfyve inhibition in combination with immune checkpoint blockade. Based on these collective findings, phase

II clinical trials of ESK981 alone (NCT03456804) or in combination with nivolumab (NCT04159896) in mCRPC are underway.

METHODS

Cell culture

VCaP, LNCaP, 22RV1, C4-2B, PC3, DU145, Renca, Myc-CaP, TRAMP-C2, B16F10, LLC, and 4T1 cell lines were obtained from ATCC. The parental LNCaP-AR cell line was provided by Charles Sawyers (Memorial Sloan Kettering Cancer Center)[60]. Enzalutamide-resistant LNCaP-AR and CWR-R1 cells were grown in RPMI-1640 supplemented with 5 or 20 μM enzalutamide, respectively. MEF *Atg5*$^{+/+}$ and *Atg5*$^{-/-}$ cells were provided by RIKEN BioResource. ID8 and Ae17 were purchased from Sigma-Aldrich; PAN02 was obtained from the NCI Division of Cancer Treatment & Diagnosis Tumor Repository. All cells were grown in 5% CO_2 incubators, regularly checked for mycoplasma, and authenticated.

Compounds

ESK981 was initially synthesized by K.D. Subsequently, ESK981 was provided by Esanik Therapeutics which licensed the compound from Teva Pharmaceuticals. Tyrosine kinase inhibitor (TKI) library (Cat.# L1800), autophagy compound library (Cat.# L2600), and other compounds were purchased from Selleckchem.

TKI library viability screening

DU145 single-cell suspensions were seeded into 96-well plates at a density of 1,000 cells/well, 16 hours prior to drug treatment. TKI library was added at 300 nM, and long-term survival was determined after 14 days of drug incubation. Viable cells were fixed with 4% formaldehyde and stained with 1% crystal violet. Percent viability was calculated by normalizing to DMSO control. Detailed screening parameters are in Supplementary Table 1.

Long-term survival assay and IC_{50} calculation

Single-cell suspensions were seeded into 96-well plates at a density of 1,000-30,000 cells/well. Long-term survival was determined after 14 days of drug incubation. Viable cells were fixed with 4% formaldehyde and stained with 1% crystal violet. IC_{50} was calculated using GraphPad Prism.

Autophagy detection for compound screening

10,000 cells were plated in 96-well plates and incubated with 300 nM of the various compounds for 24 hours. Autophagy activities were detected with CYTO-ID® Autophagy detection kit (Cat.# ENZ-KIT175, Enzo Life Sciences) according to the manufacturer's instructions, with fluorescence intensity measured on a TECAN M1000 plate reader. Autophagosome induction factor was calculated according to the manufacturer's instructions.

Autophagic flux detection

PC3 and DU145 cells were stably transfected with pMRX-IP-GFP-LC3-RFP-LC3ΔG (Addgene #84572), and single-cell clones were validated to avoid homologous recombination between the two LC3 fragments during retrovirus infection. For autophagic flux detection, 10,000 cells were plated in 96-well plates and incubated with various compounds in complete medium for 24 hours. GFP and RFP intensities were measured on a TECAN M1000 plate reader.

RNA *in situ* hybridization (ISH)

RNA ISH was performed as previously described[61]. Briefly, the RNAscope 2.5 HD BROWN Assay (Cat.# 322300; Advanced Cell Diagnostics) was used, and the target mRNA were detected by Mm-Cd3e (Cat.# 314721, Advanced Cell Diagnostics) and Mm-Cxcl10 (Cat.# 408921, Advanced Cell Diagnostics) probes. Brown punctate signals indicated positive RNA ISH staining. Positive and negative control probes, respectively, were Mm-Ppib (mouse peptidylprolyl isomerase B) and DapB (bacterial dihydrodipicolinate reductase).

Immunohistochemistry

Immunohistochemistry (IHC) was performed on FFPE tumor tissue sections using anti-Ki-67 (Cat.# 790-4286, Ventana Medical Systems). IHC was carried out using an automated protocol developed for the Benchmark XT automated slide staining system (Ventana Medical Systems) and was detected using ultraView Universal DAB detection kit (Cat.# 760-500, Ventana Medical Systems). Hematoxylin II (Cat.# 790-2208, Ventana-Roche) was used as counterstain.

Cytokine array

Cells were seeded in 6-well plates, and conditioned medium was collected after 24 hours of drug incubation. Cytokine expression was determined by proteome profiler mouse XL cytokine array (Cat.# ARY028, R&D System) or proteome profiler human XL cytokine array (Cat.# ARY022, R&D System) according to the manufacturer's instructions.

ELISA

Conditioned medium was collected after 24 hours of drug incubation. ELISA was performed using human (Cat.# KAC2361, ThermoFisher) or mouse (Cat.# ab214563, Abcam) CXCL10 ELISA kits according to the manufacturer's instructions.

Cell cycle analysis

Cells were seeded in 6-well plates and treated with various drugs for 72 hours. Single cells were fixed with 70% ethanol, stained with propidium iodine, and cell cycle was analyzed by flow cytometry.

Matrigel invasion assay

2-5×10^5 cells were seeded onto 8-μm Matrigel-coated fluoroblok transwells with serum-free medium and various concentrations of ESK981. Medium containing 10% FBS in the lower

chamber served as a chemoattractant. After 24 hours, invaded cells were stained with calcium AM green at 37°C, and fluorescence intensity was quantified with a TECAN M1000 plate reader.

3D spheroids

Nuclear RFP-expressing VCaP cells were seeded in ultralow attachment 96-well plates and spun at 1000 rpm for 10 minutes to pellet cells. Spheroids were formed after 3 days of incubation in a cell culture incubator, and then treatment was started. Red fluorescence intensity was monitored by IncuCyte ZOOM.

Yeast autophagy detection

The yeast strains used in this study were YAB499 (SEY6210, pho13Δ pho8Δ60, pdr5Δ::Kan). Antisera to Atg8 and Pgk1 were generous gifts from Dr. Jeremy Thorner (University of California, Berkeley). Protein extraction and immunoblot were performed as previously described[62]. Cells were treated with 3 μM ESK981, 3 μM cabozantinib, or the equivalent amount of DMSO as control for the indicated times.

Immunoblotting, immunofluorescence, and antibodies

Cell lysates were harvested in Pierce RIPA buffer (Thermo Scientific) containing protease (Roche) and phosphatase (Millipore) inhibitor cocktails. Protein concentrations were measured using the DC Protein Assay (Bio-Rad). Denatured lysates were separated on NuPage 4-12% Bis-Tris Midi gels (Novex) and transferred to 0.45-μm PVDF membrane (Immobilon) using a TransBlot Turbo dry transfer machine (Bio-Rad). The membrane was incubated in blocking buffer (5% non-fat dry milk, Tris-buffered saline with 0.1% Tween-20) for 1 hour at room temperature. The membrane was then incubated with the indicated antibodies for 1 hour at room temperature, followed by overnight incubation at 4°C. Chemiluminescent detection with ECL Prime (Amersham) and HyBlot CL autoradiography film (Denville Scientific) was used to visualize protein signals. Antibodies used for immunoblotting were: ATG5 (Cat.# 12994S, Cell Signaling Technology), ATG7 (Cat.# 8558S, Cell Signaling Technology), ULK1 (Cat.# 8054S, Cell Signaling Technology), Beclin1 (Cat.# 4122S, Cell Signaling Technology), FIP200 (Cat.# 12436S, Cell Signaling Technology), LC3A/B (Cat.# 12741S, Cell Signaling Technology), PIKfyve (Cat.# AF7885, R&D Systems), and GAPDH (Cat.# 3683S, Cell Signaling Technology). Antibodies were used at dilutions suggested by the manufacturers.

For LAMP1 immunofluorescence, cells were seeded on coverslips overnight and treated with 300 nM ESK981 for 24 hours. Coverslips were fixed with 10% paraformaldehyde, permeabilized with 10% saponin, blocked with 10% goat serum, and stained with LAMP1 (Cat.# 9091, Cell Signaling Technology) and fluorescently-labelled secondary antibodies. Images were obtained with a Nikon A1 confocal microscope.

For GFP-LC3 confocal imaging, GFP-LC3-expressing DU145 cells were seeded on coverslips overnight and treated with 300 nM ESK981 for various time points. Coverslips were fixed with 10% paraformaldehyde. Images were obtained with a Nikon A1 confocal microscope.

RNA isolation and quantitative real-time PCR (qPCR)

Total RNA was extracted from cells or tissue using the miRNeasy mini kit (Qiagen), and cDNA was synthesized from 1 μg total RNA using the High Capacity cDNA Reverse Transcription Kit (Applied Biosystems). qPCR was performed using Fast SYBR Green Master Mix (Applied Biosystems) on the ViiA7 Real-Time PCR System (Applied Biosystems). Target mRNA expression was quantified using the ΔΔCt method and normalized to *GAPDH*; qPCR primer sequences are listed in Supplementary Table 2.

RNA interference and short hairpin RNA

For transient knockdown experiments, cells were seeded in 6-well plates and transfected with 100 nM ON-TARGETplus Human SMARTpool siRNAs (Thermo Scientific) targeting *PIKFYVE* (Cat.# L-005058-00-0005), *PIP5K1C* (Cat.# L-004782-00-0005), *PIK3CA* (Cat.# L-003018-00-0005), or non-targeting control pool (Cat.# D-001810-10-50) using Lipofectamine® RNAiMAX (Invitrogen) according to the manufacturer's instructions. For stable doxycycline-inducible sh*Pikfyve* Myc-CaP cells, a SMARTvector lentiviral shRNA construct encoding a *Pikfyve* targeting sequence (TGGTGTCTGCGCCTAAATG) was used to infect Myc-CaP cells, and positively-infected cells were selected by puromycin.

LysoTracker Green flow cytometry analysis

Cells were grown in 6-well plates and treated with various drugs. After 24 hours, cells were stained with LysoTracker® Green DND-26 (Invitrogen), and green fluorescence signal was analyzed by flow cytometry.

Cellular thermal shift assay

The ability of compounds to interact with, and thereby stabilize the target in intact cells, was analyzed essentially as previously described[63,64]. Briefly, VCaP cells were treated with DMSO, ESK981 (1 μM), or apilimod (1 μM) for 2 hours at 37°C and 5% CO_2, and 1×10^6 single-cell suspensions were diluted into 50 μl of PBS containing protease inhibitor. Cell suspensions were then incubated in a PCR thermal cycler at various temperatures for 2 cycles of 3 minutes heating followed by 3 minutes cooling at room temperature. Cells were lysed by three cycles of freeze-thawing using liquid nitrogen. Twenty μl of the soluble fraction was analyzed by western blot.

Human prostate cancer xenograft models

The University of Michigan (U-M) Institutional Animal Care & Use Committee approved all *in vivo* studies. Four- to six-week old male CB17 severe combined immunodeficiency (SCID) mice were procured from the U-M breeding colony. Subcutaneous tumors were established at both sides of the dorsal flank. Tumors were measured biweekly at minimum using digital calipers following the formula (π/6) (L×W2), where L=length and W=width of tumors. At the end of the studies, mice were sacrificed and tumors extracted and weighed. For the VCaP castration-resistant model, 3×10^6 VCaP cells were injected in serum-free medium with 50% Matrigel (BD Biosciences). Once tumors reached ~200 mm^3, tumor-bearing mice were castrated. Once tumors grew back to the pre-castration size, mice were randomized and treated with 30 mg/kg ESK981, 60 mg/kg ESK981, or

vehicle (ORA-PLUS) by oral gavage 5 days/week. For the DU145 model, 1×10^6 DU145 cells were injected in serum-free medium with 50% Matrigel. When tumors reached ~100 mm^3, tumor-bearing mice were randomized and treated with 30 mg/kg ESK981 or vehicle (ORA-PLUS) by oral gavage 5 days/week.

Prostate patient-derived xenograft (PDX) models

The University of Texas M.D. Anderson Cancer Center PDX series has been previously described[65]. PDXs were derived from men with CRPC undergoing cystoprostatectomy[65]. MDA-PCa-146-12 and 146-10 PDX were derived from a CRPC patient diagnosed with Gleason 5+4=9 prostate adenocarcinoma. Histopathological evaluation of the cystoprostatectomy specimen demonstrated mixed prostatic adenocarcinoma and neuroendocrine carcinoma. MDA-PCa-146-12 was derived from a specimen obtained from the left bladder wall and demonstrated conventional adenocarcinoma (AR+), while MDA-PCa-146-10 was derived from the bladder wall and had neuroendocrine carcinoma morphology. PDXs were maintained in male SCID mice by surgically implanting 2 mm^3 tumors coated with 100% Matrigel to both flanks. Once tumors reached 100-200 mm^3 in size, mice were randomized and divided into different treatment groups receiving 30 mg/kg ESK981 or vehicle (ORA-PLUS) by oral gavage 5 days/week.

Syngeneic murine prostate cancer models

MYC-driven murine prostate cancer cells (Myc-CaP) were injected at a density of 1×10^6 subcutaneously into both flanks of 6-week old male FVB mice (Charles River Laboratories) in serum-free medium with 50% Matrigel. When tumors reached ~50 mm^3, tumor-bearing mice were randomized and treated with 15 mg/kg or 30 mg/kg ESK981 or vehicle (ORA-PLUS) by oral gavage 5 days/week.

For the T cell depletion study, 200 μg mouse CD4 (Cat.# BE0003-1, BioXcell), 200 μg CD8 (Cat.# BE0117, BioXcell), or 400 μg isotype control (Cat.# BE0090, BioXcell) were given 3 days prior to Myc-CaP cell injection, and dosing was maintained at 2 days/week by intraperitoneal injection (i.p.). When tumors reached ~50 mm^3, tumor-bearing mice were randomized and treated with 15 mg/kg ESK981 or vehicle by oral gavage 5 days/week.

For the ESK981 and anti-CXCR3 combination study, 15 mg/kg ESK981 or vehicle were given 5 days/week by oral gavage, while anti-CXCR3 (Cat.# BE0249, BioXcell) or isotype control (Cat.# BE0091, BioXcell) were given at 100 μg/mouse 3 times/week by i.p.

For the ESK981 and anti-PD-1 combination study, 15 mg/kg ESK981 or vehicle were given 5 days/week by oral gavage, while anti-PD-1 (Cat.# BE0146, BioXcell) or isotype control (Cat.# BE0089, BioXcell) were given at 200 μg/mouse 3 times/week by i.p.

For sh*Pikfyve* studies, Myc-CaP sh*Pikfyve* cells were injected at a density of 2×10^6 subcutaneously into both flanks of 6-week old NSG or FVB mice in serum-free medium with 50% Matrigel. When tumors reached 100 mm^3, tumor-bearing mice were randomized and treated with normal or doxycycline 625 mg/kg diet (Envigo). For the sh*Pikfyve* and anti-PD-1 combination study, when tumors reached 100 mm^3, FVB tumor-bearing mice were randomized and treated with normal or doxycycline 625 mg/kg diet for 7 days, and

then anti-PD-1 or isotype control were given at 200 μg/mouse 3 times/week in combination with normal or doxycycline diet.

Syngeneic murine breast cancer model

Breast cancer 4T1 luciferase-expressing cells were injected at a density of 0.5×10^6 subcutaneously into the right flank of 6-week old female BALB/c mice (Charles River Laboratories) in serum-free medium with 50% Matrigel. When tumors reached ~50 mm^3, tumor-bearing mice were randomized and treated with vehicle, 30 mg/kg ESK981, anti-PD-1, or ESK981 and anti-PD-1 combination. ESK981 and vehicle control were given by oral gavage 5 days/week, and anti-PD-1 or isotype control were given at 200 μg/mouse 3 days/week by i.p.

Mouse blood chemistry

Whole blood was collected using BD Microtainer SST tubes, and serum was isolated by centrifugation at 7000 rpm for 10 minutes. Sera were submitted to the U-M ULAM Pathology Cores for Animal Research for liver and renal chemistry analysis.

Flow cytometry

Mononuclear cells were isolated from the subcutaneous tumor and stained with fluorescently-conjugated antibodies as previously described[66]. Briefly, to assess cytokine production, lymphocytes were incubated in RPMI-1640 containing 10% FBS, 5 ng/ml PMA, 500 ng/ml ionomycin, Brefeldin A (1: 1000), and Monensin (1: 1000) at 37°C for 4 hours, followed by extracellular staining at 4°C for 30 minutes. Intracellular staining was performed using Foxp3/Transcription Factor Staining Buffer Set (eBioscience) under the manufacturer's protocol. Data collection and analyses were performed on a Fortessa (BD Bioscience) using BD FACS Diva software. The following antibodies were used: CD45 (Clone 30-F11, BD Biosciences), CD90.1 (Clone OX-7, BD Biosciences), CD3 (Clone 145-2C11, Thermo Fisher Scientific), CD8 (Clone 53-6.7, BD Biosciences), CD4 (Clone RM4-5, Thermo Fisher Scientific), IFNγ (Clone XMG1.2, BD Biosciences), TNFα (Clone MP6-XT22, BD Biosciences).

Transmission electron microscopy

Cells or fresh tissue were fixed with 2.5% glutaraldehyde in 0.1 M phosphate buffer, pH 7.4 for 24 hours at 4°C and then rinsed twice with 0.1 M phosphate buffer. The U-M Microscopy and Imaging core carried out sample embedding and imaging.

CRISPR *Atg5* knockout Myc-CaP cells

Guide RNAs (sgRNAs) targeting the exons of mouse *Atg5* were designed using the CRISPR Design tool (crispr.mit.edu, F. Zhang laboratory, MIT). Non-targeting sgRNA (sgNT) (forward: ACGTGGGGACATATACGTGT; reverse: ACACGTATATGTCCCCACGT) or *Atg5* targeting sgRNA (sg*Atg5*) (forward: AAGAGTCAGCTATTTGACGT; reverse: ACGTCAAATAGCTGACTCTT) were cloned into lentiCRISPRv2 plasmid, a gift from Feng Zhang (Addgene, #52961), according to published literature[67]. Myc-CaP cells were transiently transfected with the sgNT or sg*Atg5* plasmids. Post-transfection (72 hours),

cells were subjected to puromycin selection for one week. Puromycin-resistant cells were resuspended into single cells and seeded into 96-well plates. One month later, *Atg5* knockout clones were screened by western blot.

Gene expression analysis

RNA was extracted from cell lines or tissue using the QIAGEN RNA extraction kit. RNA quality was determined by the Bioanalyzer RNA Nano Chip. Myc-CaP xenograft tumors used the RiboErase selection kit (Cat.# KK8561, Kapa Biosystems), while the remaining samples used poly-A selection by Sera-Mag™ Oligo(dT)-Coated Magnetic Particles (Cat.# 38152103010150, GE Healthcare Life Sciences), and libraries were generated by KAPA RNA HyperPrep Kit (Cat.# KK8541, Roche Sequencing Solutions). RNA-sequencing was performed on the Illumina HiSeq™ 2500. Reads were aligned with the Spliced Transcripts Alignment to a Reference (STAR) to the mouse reference genome mm10[68]. Principal Component Analysis (PCA) was performed on variance-stabilizing transformation (vst) of read-count data using DESeq2[69]. Gene differential expression analysis was carried out with edgeR[70]. Mouse gene set enrichment analysis (GSEA) was performed with WebGestalt analysis web tool at http://www.webgestalt.org.

Lipidomics

Details of sample preparation and identification for untargeted lipidomic profiling have been previously reported[71]. Lipids were extracted using a modified Bligh-Dyer method[72]. Extraction was carried out using a 2:2:2 volume ratio of water:methanol:dichloromethane at room temperature after spiking internal standard lipids (17:0LPC, 17:0PC, 17:0PE, 17:0PG, 17:0 ceramide, 17:0SM, 17:0PS, 17:0PA, 17:0TG, 17:0MG, d5-DG, d31-TG, and 17.0-20.4 PI). The organic layer was collected and dried completely under nitrogen. The organic dried extract containing lipids was further analyzed by liquid chromatography-mass spectrometry (MS)-based lipidomics. The dried lipid extracts were injected onto a 1.8-μm particle 50×2.1 mm id Waters Corporation Acquity HSS T3 column, which was heated to 55°C. A binary gradient system consisting of acetonitrile and water with 10 mM ammonium acetate (40:60, v:v) was used as eluent A. Eluent B consisted of water, acetonitrile, and isopropanol, both containing 10 mM ammonium acetate (5:10:85, v:v:v). The lipid extracts were reconstituted with a buffer B and injected to MS. The MS analysis alternated between MS and data-dependent MS2 scans using dynamic exclusion in both positive and negative polarity. As controls (QC) to monitor the profiling process, a pool of plasma and test plasma (a small aliquot from all test samples) were extracted and analyzed in tandem with experimental samples. These controls were incorporated multiple times into the randomization scheme such that sample preparation and analytical variability could be constantly monitored. Lipids were identified using LIPIDBLAST library[73] (computer-generated tandem mass spectral library of 212,516 spectra covering 119,200 compounds from 26 lipid compound classes) by matching the product ion's MS/MS data. MS data files were processed using MultiQuant 1.1.0.26 (Applied Biosystems/MDS Analytical Technologies). Identified lipids were quantified by normalizing against their respective internal standard. QC samples were used to monitor the overall quality of the lipid extraction and MS analyses and were mainly used to remove technical outliers and lipid species that were detected below the lipid class-based lower limit of quantification.

Lipid kinase competition assay

Lipid kinase competition assays for 22 lipid kinases, including clinically-relevant mutants, were performed using DiscoveRX KINOEscan® platform scanLIPID® panel. Detailed information is described on the DiscoveRX website (https://www.discoverx.com/technologies-platforms/competitive-binding-technology/kinomescan-technology-platform).

Kinase dissociation constant analysis

Quantitative binding constants (Kd) of ESK981 to PIKfyve, PIP5K1A, PIP5K1C, and PIK3CA were generated using KdELECT® platform (DiscoveRX). An 11-point dose-response of ESK981 (0.05-3000 nM) was used. Detailed information is provided on the DiscoveRX website (https://www.discoverx.com).

Further information on research design is available in the *Nature* Research Reporting Summary linked to this article.

Statistics and reproducibility

No data were excluded from the analyses. No statistical method was used to predetermine sample size. For all *in vivo* experiments, animals were randomly assigned to a treatment group after tumor inoculation. The starting tumor burden in the treatment and control groups was similar before treatment. For *in vitro* experiments, all samples were analyzed equally with no sub-sampling, and, therefore, there was no requirement for randomization. For *in vivo* experiments, tumor measurement by digital caliper was performed in a blinded manner. *In vitro* experiments were not performed in a blinded manner as the investigator needed to know the treatment groups in order to complete the study. Statistical analysis was performed using a two-tailed, unpaired t test, unless otherwise indicated in figure legends. Figure legends also denote that error bars indicate the mean ± SEM. GraphPad Prism software (version 8) and R v.3.6.0 were used for statistical calculations.

Extended Data

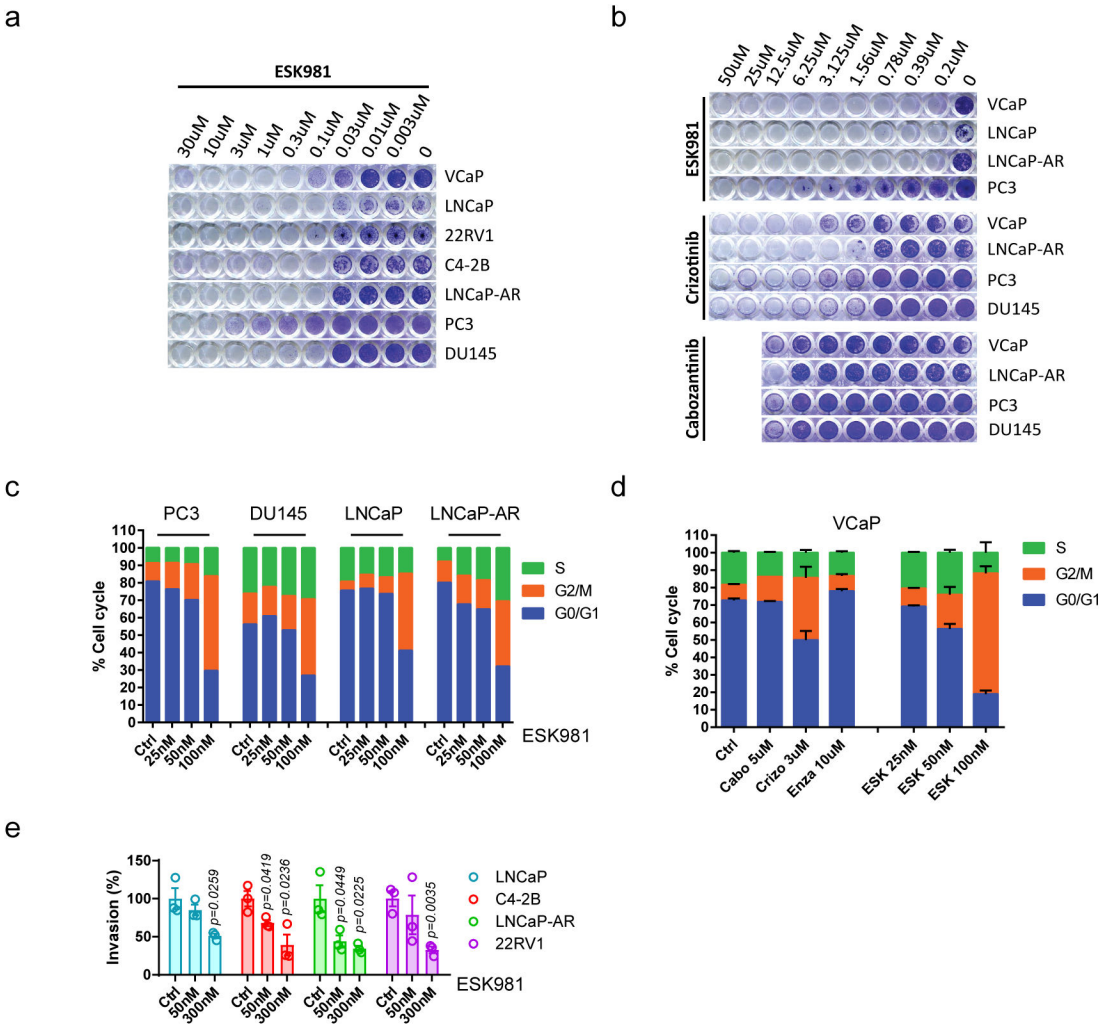

Extended Data Fig. 1. ESK981 blocks cell growth, induces cell cycle arrest, and decreases cellular invasion.

(a-b) Representative crystal violet staining for a long-term survival assay of a panel of prostate cell lines at various concentrations of ESK981, crizotinib, or cabozantinib.

(c) Cell cycle analysis was measured after 72 hours of increasing concentrations of ESK981 treatment in indicated prostate cancer cell lines. Ctrl, control.

(d) Cell cycle analysis of VCaP cells that were treated with the indicated compounds for 72 hours. Cabo, cabozantinib; Crizo, crizotinib; Enza, enzalutamide; ESK, ESK981.

(e) Matrigel invasion assay of various prostate cancer cell lines that were treated with the indicated concentrations of ESK981. The percentage invasion was quantified with a fluorescent plate reader. Data were analyzed by two-tailed unpaired t test from three independent experiments and presented as mean ± SEM. P-value indicated.

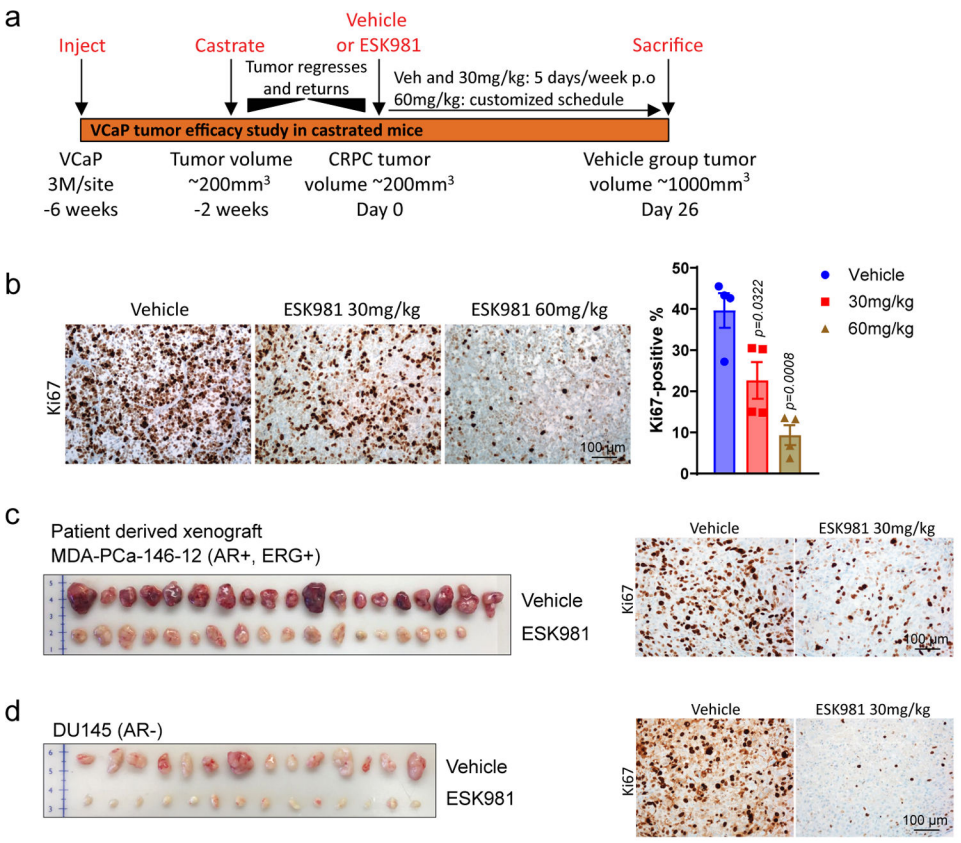

Extended Data Fig. 2. ESK981 inhibits the growth of diverse preclinical models of prostate cancer in vivo.

(a) Schematic illustration of the VCaP CRPC mouse xenograft experimental design. To generate castration-resistant VCaP, parental VCaP cells were injected subcutaneously into both flanks of intact male mice. When average VCaP tumors reached 200 mm^3, mice were surgically castrated and VCaP tumors regressed due to loss of androgen. Castration-resistant VCaP tumors developed as VCaP tumors grew back to the size of pre-castration. Castration-resistant VCaP tumors were then randomized into three groups and treated with vehicle, 30 mg/kg, or 60 mg/kg ESK981 p.o., oral gavage.

(b) Representative IHC images for proliferation marker Ki67 are shown after treatment with the indicated drugs for five days in VCaP tumors (left). Quantification of positive Ki67 percentage is shown on the right (right). Data were analyzed by two-tailed unpaired t test and presented as mean ± SEM. N=4 tumors per group. P-value indicated.

(c) Representative individual tumors from vehicle and ESK981 groups in AR^+ and ERG^+ prostate PDX MDA-PCa-146-12 (left). Representative IHC showing Ki67 staining for vehicle and 30 mg/kg ESK981 groups of MDA-PCa-146-12 tumors (right) from three independent experiments.

(d) Representative individual tumors from vehicle and ESK981 groups of DU145 tumors (left). Representative IHC showing Ki67 staining for the vehicle and 30 mg/kg ESK981 groups of DU145 tumors (right) from three independent experiments.

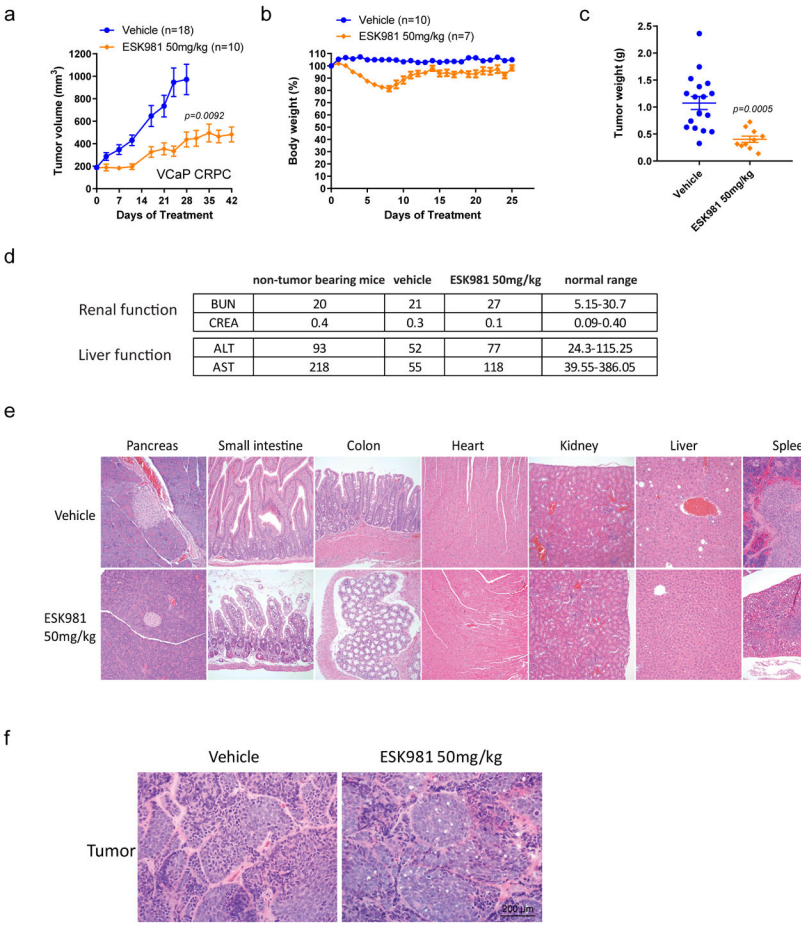

Extended Data Fig. 3. Renal function, liver function, and histopathological evaluation of ESK981-treated xenografts.

(a) Castration-resistant VCaP tumors were established according to Extended Data Fig. 2a. Tumor-bearing mice were divided into vehicle and ESK981 50 mg/kg groups, and tumor volumes were monitored twice per week for six weeks. Data were analyzed by two-tailed unpaired t test and presented as mean ± SEM at day 25. N=number of tumors and P-value indicated.

(b) The percent body weights of VCaP tumor-bearing mice were monitored daily throughout this study. Data were presented as mean ± SEM. N=number of mice.

(c) The weight of VCaP tumors from vehicle (n=18 tumors) and ESK981 50 mg/kg (n=10 tumors) were measured at the end of this study. Data were analyzed by two-tailed unpaired t test and presented as mean ± SEM. P-value indicated.

(d) Blood chemistry was evaluated for renal and liver functions in non-tumor-bearing and VCaP tumor-bearing mice in vehicle and 50 mg/kg ESK981 treatment groups.

(e) Representative histological sections showing H&E staining for various organs taken from vehicle- or ESK981-treated mice from three independent experiments.

(f) Representative histological sections showing H&E staining for tumors taken from vehicle- or ESK981-treated mice from three independent experiments.

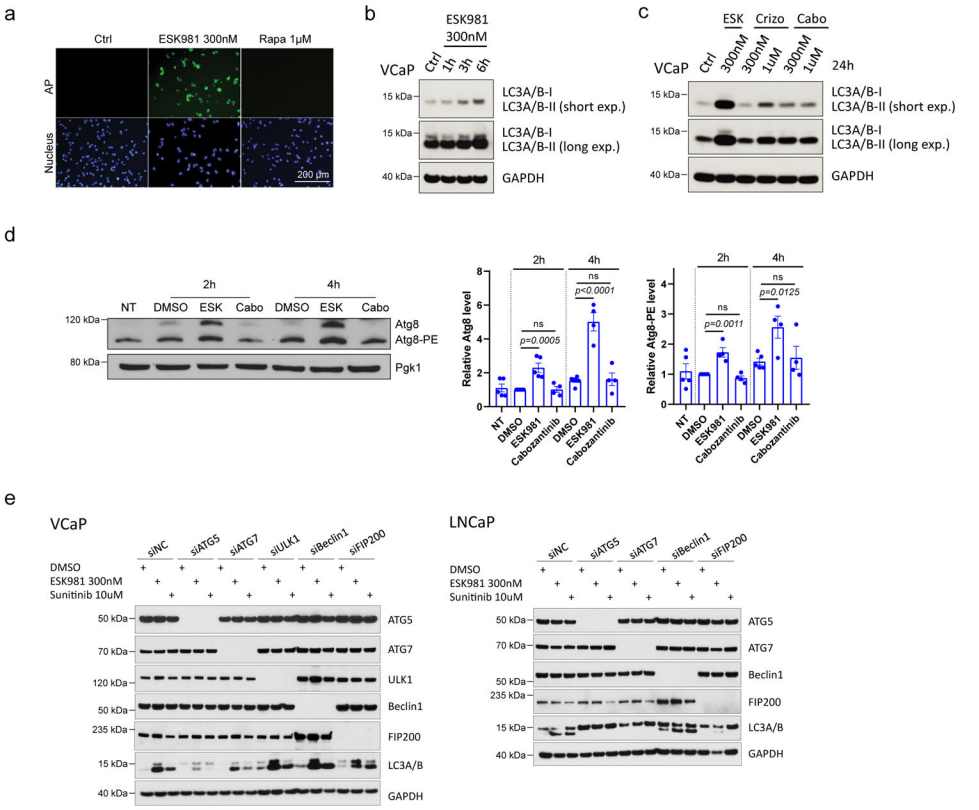

Extended Data Fig. 4. ESK981 robustly induces autophagosome levels and is dependent on ATG5 for its effects.

(a) DU145 cells with the indicated drug treatment for 24 hours. Autophagosome induction activity was visualized by CYTO-ID® assay from three independent experiments. Rapa, rapamycin.

(b) VCaP cells were treated with 300 nM ESK981 for the indicated time points, and LC3 protein levels were assessed by western blot from three independent experiments.

(c) VCaP cells were treated with ESK981 (ESK), crizotinib (Crizo), and cabozantinib (Cabo) at the indicated concentrations. Protein levels of LC3 were examined after 24 hours of treatment from three independent experiments.

(d) Protein levels of Atg8 in yeast *prd5Δ* cells after ESK981 (ESK) or cabozantinib (Cabo) treatment under nitrogen deprivation conditions. NT, no treatment. Data were analyzed by two-tailed unpaired t test from four independent experiments and presented as mean ± SEM. P value indicated.

(e) Protein levels of indicated protein post various siRNA knockdown in VCaP and LNCaP cells with or without 300 nM ESK981 or 1 μM sunitinib treatment for 24 hours from three independent experiments.

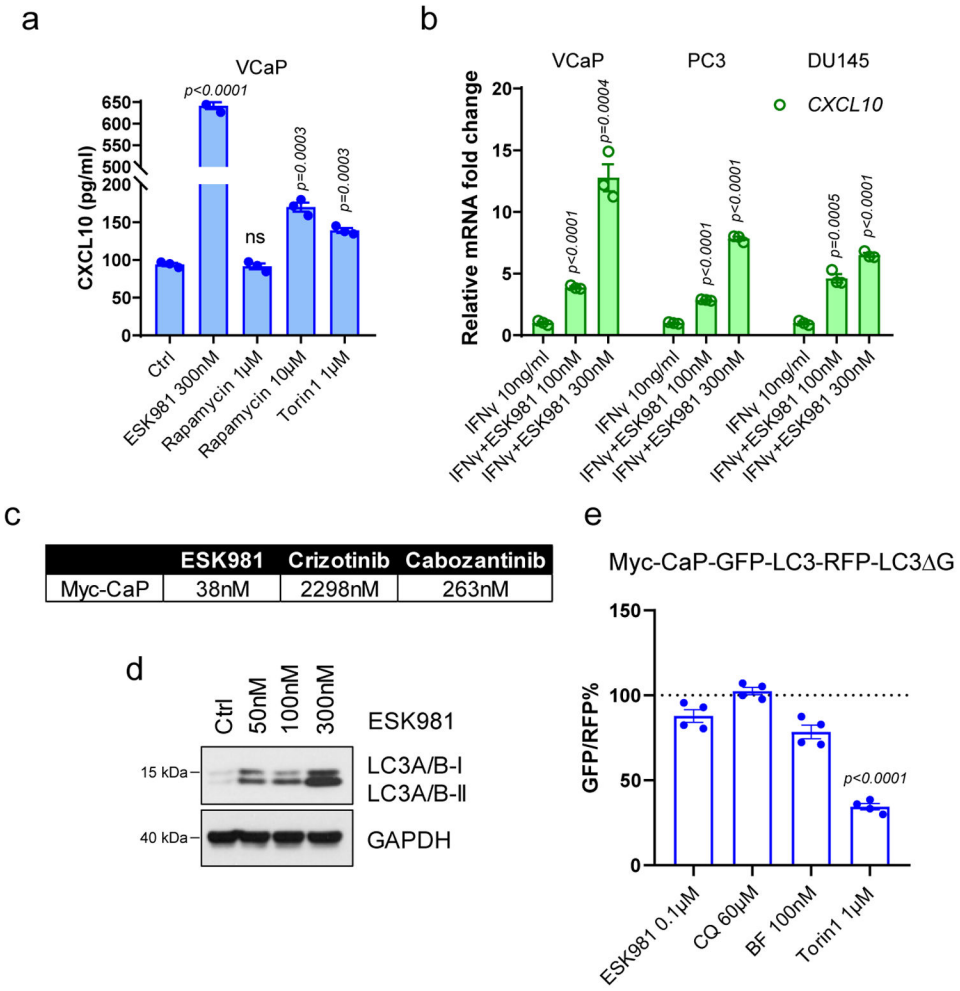

Extended Data Fig. 5. ESK981 upregulates CXCL10 expression in human prostate cancer cells and inhibits autophagy in murine Myc-CaP prostate cancer cells.

(a) CXCL10 protein levels measured by ELISA in conditioned media from VCaP cells treated with ESK981 or various autophagy inducers for 24 hours. Data were analyzed by two-tailed unpaired t test from three independent experiments and presented as mean ± SEM. P-value indicated.

(b) *CXCL10* mRNA levels measured by quantitative PCR (qPCR) in VCaP, PC3, and DU145 cells with the indicated treatment for 24 hours. IFNγ, interferon gamma. Data were analyzed by two-tailed unpaired t test from three independent experiments and presented as mean ± SEM. P-value indicated.

(c) IC_{50} of ESK981, crizotinib, and cabozantinib determined in Myc-CaP cells.

(d) Protein levels of LC3 after 50 nM, 100 nM, and 300 nM ESK981 treatment for 24 hours in Myc-CaP cells from three independent experiments.

(e) Ratio of GFP/RFP signal in Myc-CaP GFP-LC3-RFP-LC3ΔG stable expressing cells with the indicated treatment for 24 hours. Data were analyzed by two-tailed unpaired t test from four independent experiments and presented as mean ± SEM. P-value indicated.

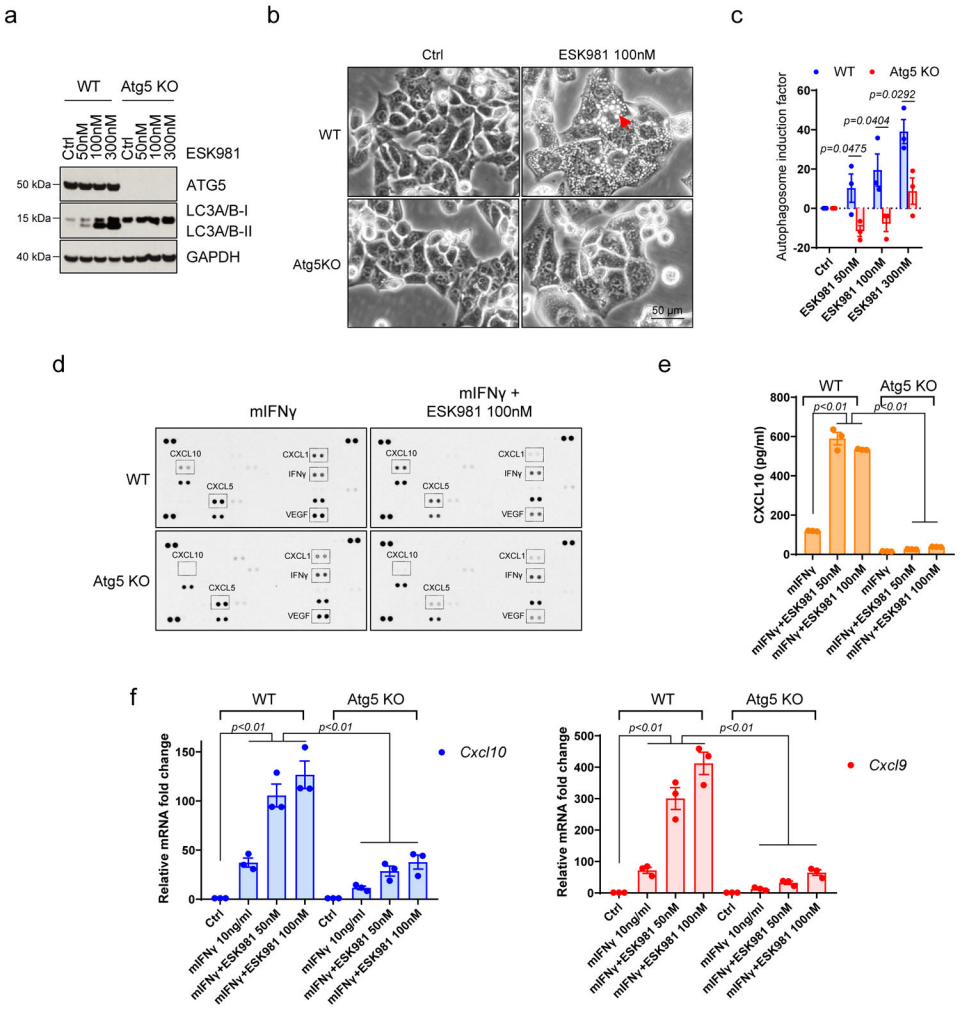

Extended Data Fig. 6. Atg5 deletion blocks ESK981-induced vacuolization and CXCL10-mediated immune response.

(a) Myc-CaP wild-type (WT) and *Atg5* knockout (*Atg5* KO) cells were treated with increasing concentrations of ESK981 for 24 hours. Atg5 and LC3 levels were assessed by western blot from three independent experiments. GAPDH served as a loading control.

(b) Representative morphology of vacuolization in Myc-CaP wild-type (WT) and *Atg5* knockout (*Atg5* KO) cells after treatment with control or 100 nM ESK981 for 24 hours from three independent experiments.

(c) Autophagosome content of Myc-CaP WT and *Atg5* KO cells were measured by CYTO-ID® assay after being treated with increasing concentrations of ESK981 for 24 hours. Data were analyzed by two-tailed unpaired t test from three independent experiments and presented as mean ± SEM. P-value indicated.

(d) Mouse cytokine array using Myc-CaP WT and *Atg5* KO cell supernatant after treatment with 10 ng/ml mouse interferon gamma (mIFNγ) or mIFNγ + 100 nM ESK981 for 24 hours. Differential expression candidate dots are highlighted by boxes.

(e) Mouse CXCL10 protein levels were measured by ELISA in Myc-CaP WT and *Atg5* KO conditioned medium with the indicated treatment for 24 hours. Data were analyzed

by two-tailed unpaired t test from three independent experiments and presented as mean ± SEM. P-value indicated.

(f) mRNA levels of *Cxcl10* and *Cxcl9* were measured by qPCR in Myc-CaP WT and *Atg5* KO cells with 50 nM or 100 nM ESK981 and 10 ng/ml mIFNγ treatment for 24 hours. Data were analyzed by two-tailed unpaired t test from three independent experiments and presented as mean ± SEM. P-value indicated.

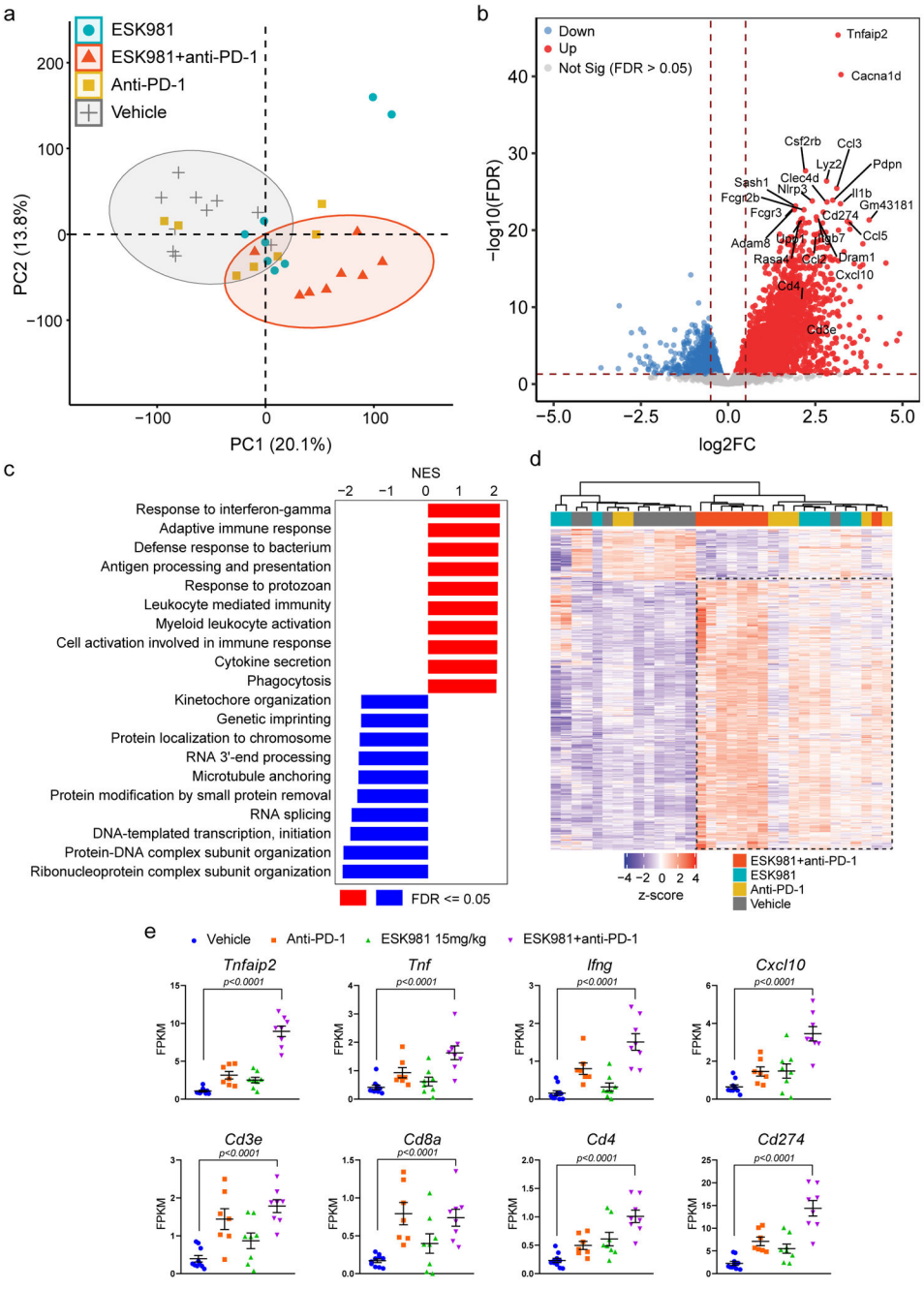

Extended Data Fig. 7. Transcriptomic analysis of Myc-CaP tumors treated with ESK981 in combination with anti-PD-1 immunotherapy in FVB mice.

(a) Principal Component Analysis (PCA) of individual Myc-CaP tumors from indicated treatment groups based on variance-stabilizing transformation (vst) of read-count data. The vehicle and ESK981+anti-PD-1 combination groups form a relatively distinct cluster based on the first two principal components.
(b) Volcano plot of differential gene expression analysis for groups treated with ESK981+anti-PD-1 versus vehicle. The horizontal dashed line corresponds to the FDR = 0.05. The vertical dashed lines correspond to log2FC >= 1 (up-regulation) or log2FC <= −1 (down-regulation).
(c) Mouse Gene Set Enrichment Analysis (GSEA) with biological process gene ontology for groups treated with ESK981+anti-PD-1 versus vehicle. Top 10 gene sets are ordered by normalized enrichment score (NES). The top enriched categories are relevant to immune responses and inflammation.
(d) Heatmap representation of top differentially expressed genes in groups treated with ESK981+anti-PD-1 versus vehicle (FDR <= 0.01, up or down-regulated by at least 2-fold).
(e) Fragments per kilobase of exon model per million reads mapped (FPKM) of indicated targets from individual Myc-CaP tumors treated with vehicle (n=10 tumors), ESK981 (n=8 tumors), anti-PD-1 (n=7 tumors), or ESK981+anti-PD-1 (n=8 tumors). Data were analyzed by two-tailed unpaired t test and presented as mean ± SEM. P-value indicated.

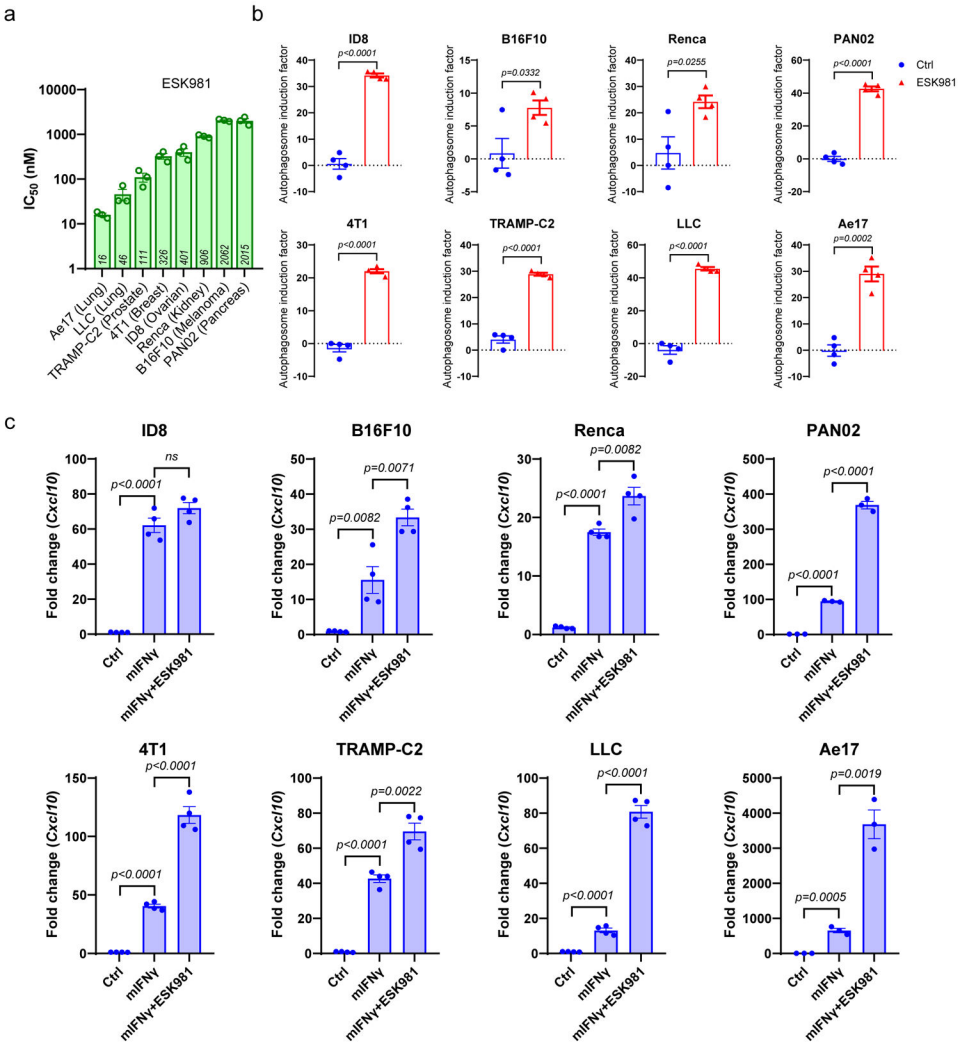

Extended Data Fig. 8. ESK981 induces autophagosome formation and upregulates Cxcl10 expression in various murine cancer cell lines.

(a) IC_{50} from cell viability assays of ESK981 in murine cancer cells of lung (Ae17, LLC), melanoma (B16F10), ovarian (ID8), pancreas (PAN02), renal (Renca), prostate (TRAMP-C2), and breast (4T1) lineages. Data were plotted as mean ± SEM from three independent experiments.

(b) Autophagosome content measured by CYTO-ID in indicated cell lines treated with control (Ctrl) or 300 nM ESK981 for 24 hours. Data were analyzed by two-tailed unpaired t test from four independent experiments and presented as mean ± SEM. P-value indicated.

(c) mRNA level of *Cxcl10* in indicated cell lines treated with 10 ng/ml mIFNγ or mIFNγ plus 300 nM ESK981 for 24 hours. Data were analyzed by two-tailed unpaired t test from three (PAN02, Ae17) or four (ID8, B16F10, Renca, 4T1, TRAMP-C2, LLC) independent experiments and presented as mean ± SEM. P-value indicated.

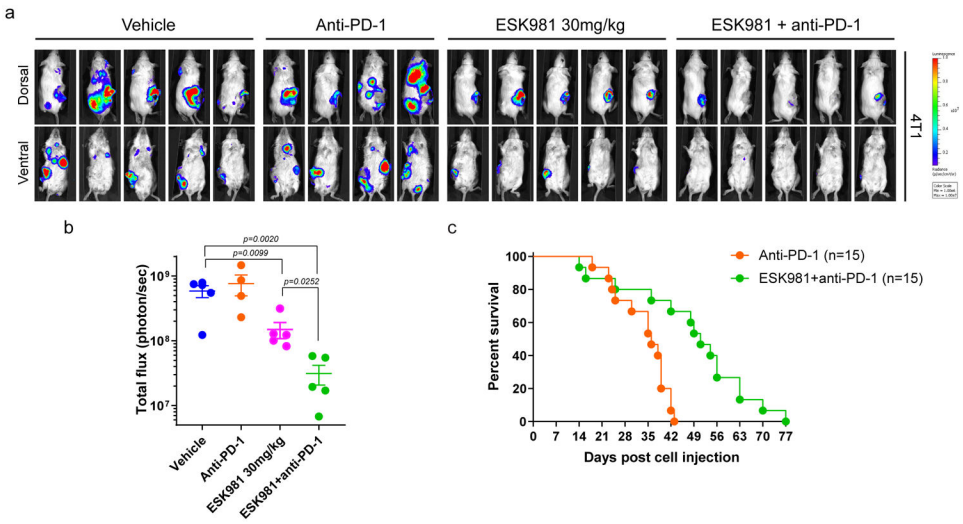

Extended Data Fig. 9. ESK981 sensitizes the murine breast cancer 4T1 model to anti-PD-1 immunotherapy.

(a) Bioluminescent signaling images showing dorsal and ventral views of individual 4T1 tumor-bearing mice from indicated treatment groups.

(b) Bioluminescent quantification of total tumor burden from individual mice treated with vehicle (n=5 mice), anti-PD-1 (n=4 mice), ESK981 15 mg/kg (n=5 mice), ESK981+anti-PD-1 (n=5 mice). Data were analyzed by two-tailed unpaired t test and presented as mean ± SEM. P-value indicated.

(c) Overall survival of 4T1-bearing mice treated with either anti-PD-1 (n=15 mice) or ESK981 and anti-PD-1 combination (n=15 mice).

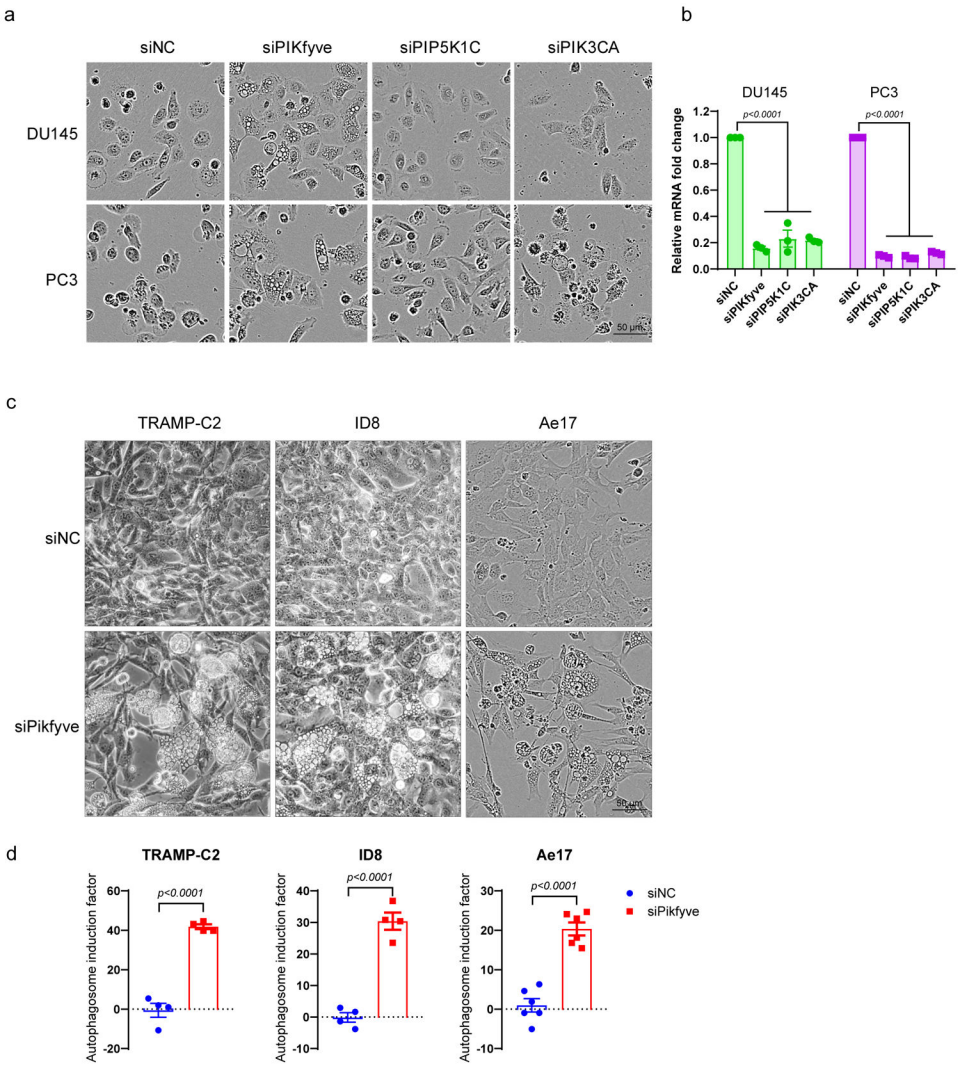

Extended Data Fig. 10. PIKfyve mediates a cellular vacuolization morphology in human prostate cancer cells and murine cancer cells, and Pikfyve loss induces accumulation of autophagosomes in various murine cancer cells.

(a) Morphology of DU145 and PC3 cells after siNC, si*PIKFYVE*, si*PIP5K1C*, or si*PIK3CA* transfection from three independent experiments.

(b) mRNA levels of *PIKFYVE*, *PIP5K1C*, and *PIK3CA* were measured by qPCR after siRNA knockdown of indicated targets in DU145 and PC3 cells. Data were analyzed by two-tailed unpaired t test and presented as mean ± SEM from three independent experiments. P-value indicated.

(c) Morphological changes of TRAMP-C2, ID8, and Ae17 cells after siNC or si*Pikfyve* transfection from three independent experiments.

(d) Autophagosome induction activity measured with CYTO-ID® assay in TRAMP-C2, ID8, and Ae17 cells after siRNA knockdown of *Pikfyve*. Data were analyzed by two-tailed unpaired t test and presented as mean ± SEM from four (TRAMP-C2 and ID8) and six (Ae17) independent experiments. P-value indicated.

Supplementary Material

Refer to Web version on PubMed Central for supplementary material.

ACKNOWLEDGEMENTS

The authors would like to thank Mandy Trierweiler and Sylvia Zelenka-Wang for histological sample processing and immunohistochemistry as well as undergraduate student Kaelie Johnson for technical assistance. This work was supported by a Prostate Cancer Foundation (PCF) Challenge Award, NCI Prostate SPORE Grant P50CA186786, Department of Defense (DoD) PC130151P1 (N.N. and A.M.C.), and NIH grant GM131919 (D.J.K.). A.M.C. is an NCI Outstanding Investigator (R35CA231996), Howard Hughes Medical Institute Investigator, A. Alfred Taubman Scholar, and American Cancer Society Professor. Y.Q. and J.C.T. are supported by PCF Young Investigator Awards. L.X. is supported by a DoD Postdoctoral Award (W81XWH-16-1-0195). E.L.E. was supported by the Academy of Finland.

Data availability

Raw RNA sequencing data are deposited at the NCBI Gene Expression Omnibus (GSE174644). Further information and requests for resources and reagents should be directed to the corresponding author. All requests for raw and analyzed data and materials will be promptly reviewed by the corresponding authors to verify if the request is subject to any intellectual property or confidentiality obligations. Any data and materials that can be shared will be released via a Material Transfer Agreement. Source data have been provided with this paper for Figs. 1-8 as well as Extended Data Figs. 1-10.

REFERENCES

1. Ferraldeschi R, Welti J, Luo J, Attard G & de Bono JS Targeting the androgen receptor pathway in castration-resistant prostate cancer: progresses and prospects. Oncogene 34, 1745–1757 (2015). [PubMed: 24837363]
2. Scher HI, et al. Increased survival with enzalutamide in prostate cancer after chemotherapy. N. Engl. J. Med 367, 1187–1197 (2012). [PubMed: 22894553]
3. de Bono JS, et al. Abiraterone and increased survival in metastatic prostate cancer. N. Engl. J. Med 364, 1995–2005 (2011). [PubMed: 21612468]
4. Qiao Y, et al. Mechanistic support for combined MET and AR blockade in castration-resistant prostate cancer. Neoplasia 18, 1–9 (2016). [PubMed: 26806347]
5. Ahronian LG & Corcoran RB Strategies for monitoring and combating resistance to combination kinase inhibitors for cancer therapy. Genome Med. 9, 1–12 (2017). [PubMed: 28081715]
6. Smith DC, et al. Cabozantinib in patients with advanced prostate cancer: results of a phase II randomized discontinuation trial. J. Clin. Oncol 31, 412–419 (2013). [PubMed: 23169517]
7. Smith M, et al. Phase III study of cabozantinib in previously treated metastatic castration-resistant prostate cancer: COMET-1. J. Clin. Oncol 34, 3005–3013 (2016). [PubMed: 27400947]
8. Hudkins RL, et al. Synthesis and biological profile of the pan-vascular endothelial growth factor receptor/tyrosine kinase with immunoglobulin and epidermal growth factor-like homology domains 2 (VEGF-R/TIE-2) inhibitor 11-(2-methylpropyl)-12,13-dihydro-2-methyl-8-(pyrimidin-2-ylamino)-4H-indazolo[5, 4-a]pyrrolo[3,4-c]carbazol-4-one (CEP-11981): a novel oncology therapeutic agent. J. Med. Chem. 55, 903–913 (2012). [PubMed: 22148921]
9. Pili R, Carducci M, Brown P & Hurwitz H An open-label study to determine the maximum tolerated dose of the multitargeted tyrosine kinase inhibitor CEP-11981 in patients with advanced cancer. Invest. New Drugs 32, 1258–1268 (2014). [PubMed: 25152243]
10. Shisheva A PIKfyve: Partners, significance, debates and paradoxes. Cell Biol. Int 32, 591–604 (2008). [PubMed: 18304842]

11. Gayle S, et al. Identification of apilimod as a first-in-class PIKfyve kinase inhibitor for treatment of B-cell non-Hodgkin lymphoma. Blood 129, 1768–1778 (2017). [PubMed: 28104689]
12. Baird AM, et al. IL-23R is epigenetically regulated and modulated by chemotherapy in non-small cell lung cancer. Front. Oncol 3, 162 (2013). [PubMed: 23802098]
13. Bonolo De Campos C, et al. Identification of PIKfyve kinase as a target in multiple myeloma. Haematologica 105, 1641–1649 (2019). [PubMed: 31582538]
14. Levy JMM, Towers CG & Thorburn A Targeting autophagy in cancer. Nat. Rev. Cancer 17, 528–542 (2017). [PubMed: 28751651]
15. Noman MZ, et al. Inhibition of Vps34 reprograms cold into hot inflamed tumors and improves anti-PD-1/PD-L1 immunotherapy. Sci. Adv 6, eaax7881 (2020). [PubMed: 32494661]
16. Mgrditchian T, et al. Targeting autophagy inhibits melanoma growth by enhancing NK cells infiltration in a CCL5-dependent manner. Proc. Natl. Acad. Sci. U.S.A 114, E9271–E9279 (2017). [PubMed: 29078276]
17. Wei H, et al. Suppression of autophagy by FIP200 deletion inhibits mammary tumorigenesis. Genes Dev 25, 1510–1527 (2011). [PubMed: 21764854]
18. Yamamoto K, et al. Autophagy promotes immune evasion of pancreatic cancer by degrading MHC-I. Nature 581, 100–105 (2020). [PubMed: 32376951]
19. Beer TM, et al. Randomized, double-blind, phase III trial of ipilimumab versus placebo in asymptomatic or minimally symptomatic patients with metastatic chemotherapy-naive castration-resistant prostate cancer. J. Clin. Oncol 35, 40–47 (2017). [PubMed: 28034081]
20. Kwon ED, et al. Ipilimumab versus placebo after radiotherapy in patients with metastatic castration-resistant prostate cancer that had progressed after docetaxel chemotherapy (CA184-043): a multicentre, randomised, double-blind, phase 3 trial. Lancet Oncol. 15, 700–712 (2014). [PubMed: 24831977]
21. Wheeler DL, Iida M & Dunn EF The role of Src in solid tumors. Oncologist 14, 667–678 (2009). [PubMed: 19581523]
22. Nagasawa J, et al. Novel HER2 selective tyrosine kinase inhibitor, TAK-165, inhibits bladder, kidney and androgen-independent prostate cancer in vitro and in vivo. Int. J. Urol 13, 587–592 (2006). [PubMed: 16771730]
23. Harshman LC, et al. An investigator-initiated phase I study of crizotinib in combination with enzalutamide in metastatic castration-resistant prostate cancer (mCRPC) before or after progression on docetaxel. J. Clin. Oncol 34, e16509 (2016).
24. Tripathi A, et al. Dual blockade of c-MET and the androgen receptor in metastatic castration-resistant prostate cancer: a phase I study of concurrent enzalutamide and crizotinib. Clin. Cancer Res 26, 6122–6131 (2020). [PubMed: 32943461]
25. Hickman JA, et al. Three-dimensional models of cancer for pharmacology and cancer cell biology: capturing tumor complexity in vitro/ex vivo. Biotechnol. J 9, 1115–1128 (2014). [PubMed: 25174503]
26. Harma V, et al. A comprehensive panel of three-dimensional models for studies of prostate cancer growth, invasion and drug responses. PloS one 5, e10431 (2010). [PubMed: 20454659]
27. Robinson D, et al. Integrative clinical genomics of advanced prostate cancer. Cell 161, 1215–1228 (2015). [PubMed: 26000489]
28. Yang ZJ, Chee CE, Huang S & Sinicrope FA The role of autophagy in cancer: therapeutic implications. Mol. Cancer Ther 10, 1533–1541 (2011). [PubMed: 21878654]
29. Klionsky DJ, et al. Guidelines for the use and interpretation of assays for monitoring autophagy (3rd edition). Autophagy 12, 1–222 (2016). [PubMed: 26799652]
30. Marx V Autophagy: eat thyself, sustain thyself. Nat. Methods 12, 1121–1125 (2015). [PubMed: 26624796]
31. Kim J & Klionsky DJ Autophagy, cytoplasm-to-vacuole targeting pathway, and pexophagy in yeast and mammalian cells. Annu. Rev. Biochem 69, 303–342 (2000). [PubMed: 10966461]
32. Miller WT Tyrosine kinase signaling and the emergence of multicellularity. Biochim. Biophys. Acta 1823, 1053–1057 (2012). [PubMed: 22480439]

33. Kaizuka T, et al. An autophagic flux probe that releases an internal control. Mol. Cell 64, 835–849 (2016). [PubMed: 27818143]
34. Poillet-Perez L, et al. Autophagy maintains tumour growth through circulating arginine. Nature 563, 569–573 (2018). [PubMed: 30429607]
35. Kraya AA, et al. Identification of secreted proteins that reflect autophagy dynamics within tumor cells. Autophagy 11, 60–74 (2015). [PubMed: 25484078]
36. Liu M, Guo S & Stiles JK The emerging role of CXCL10 in cancer. Oncol. Lett 2, 583–589 (2011). [PubMed: 22848232]
37. Harlin H, et al. Chemokine expression in melanoma metastases associated with CD8+ T-cell recruitment. Cancer Res. 69, 3077–3085 (2009). [PubMed: 19293190]
38. Bronger H, et al. CXCL9 and CXCL10 predict survival and are regulated by cyclooxygenase inhibition in advanced serous ovarian cancer. Br. J. Cancer 115, 553–563 (2016). [PubMed: 27490802]
39. Tokunaga R, et al. CXCL9, CXCL10, CXCL11/CXCR3 axis for immune activation - a target for novel cancer therapy. Cancer Treat. Rev 63, 40–47 (2018). [PubMed: 29207310]
40. Watson PA, et al. Context-dependent hormone-refractory progression revealed through characterization of a novel murine prostate cancer cell line. Cancer Res. 65, 11565–11571 (2005). [PubMed: 16357166]
41. Serganova I, et al. Enhancement of PSMA-directed CAR adoptive immunotherapy by PD-1/PD-L1 blockade. Mol. Ther. Oncolytics 4, 41–54 (2017). [PubMed: 28345023]
42. Rockenfeller P, et al. Phosphatidylethanolamine positively regulates autophagy and longevity. Cell Death Differ. 22, 499–508 (2015). [PubMed: 25571976]
43. Sharma G, et al. A family of PIKFYVE inhibitors with therapeutic potential against autophagy-dependent cancer cells disrupt multiple events in lysosome homeostasis. Autophagy 15, 1694–1718 (2019). [PubMed: 30806145]
44. Gayle S, et al. B-cell non-Hodgkin lymphoma: Selective vulnerability to PIKFYVE inhibition. Autophagy 13, 1082–1083 (2017). [PubMed: 28350209]
45. Efe JA, Botelho RJ & Emr SD The Fab1 phosphatidylinositol kinase pathway in the regulation of vacuole morphology. Curr. Opin. Cell Biol 17, 402–408 (2005). [PubMed: 15975782]
46. Ciciola P, Cascetta P, Bianco C, Formisano L & Bianco R Combining immune checkpoint inhibitors with anti-angiogenic agents. J. Clin. Med 9(2020).
47. Sbrissa D, Ikonomov OC & Shisheva A PIKfyve, a mammalian ortholog of yeast Fab1p lipid kinase, synthesizes 5-phosphoinositides. Effect of insulin. J. Biol. Chem 274, 21589–21597 (1999). [PubMed: 10419465]
48. Jefferies HB, et al. A selective PIKfyve inhibitor blocks PtdIns(3,5)P(2) production and disrupts endomembrane transport and retroviral budding. EMBO Rep. 9, 164–170 (2008). [PubMed: 18188180]
49. Choy CH, et al. Lysosome enlargement during inhibition of the lipid kinase PIKfyve proceeds through lysosome coalescence. J. Cell Sci 131(2018).
50. Nguyen HG, et al. Targeting autophagy overcomes enzalutamide resistance in castration-resistant prostate cancer cells and improves therapeutic response in a xenograft model. Oncogene 33, 4521–4530 (2014). [PubMed: 24662833]
51. Yang S, et al. Pancreatic cancers require autophagy for tumor growth. Genes Dev. 25, 717–729 (2011). [PubMed: 21406549]
52. Saleem A, et al. Effect of dual inhibition of apoptosis and autophagy in prostate cancer. The Prostate 72, 1374–1381 (2012). [PubMed: 22241682]
53. Santanam U, et al. Atg7 cooperates with Pten loss to drive prostate cancer tumor growth. Genes Dev. 30, 399–407 (2016). [PubMed: 26883359]
54. Poillet-Perez L, et al. Autophagy promotes growth of tumors with high mutational burden by inhibiting a T-cell immune response. Nat. Cancer 1, 923–934 (2020). [PubMed: 34476408]
55. Antonarakis ES, et al. Pembrolizumab for treatment-refractory metastatic castration-resistant prostate cancer: multicohort, open-label phase II KEYNOTE-199 study. J. Clin. Oncol 38, 395–405 (2020). [PubMed: 31774688]

56. Abida W, et al. Analysis of the prevalence of microsatellite instability in prostate cancer and response to immune checkpoint blockade. JAMA Oncol. 5, 471–478 (2019). [PubMed: 30589920]
57. Antonarakis ES, et al. Clinical features and therapeutic outcomes in men with advanced prostate cancer and DNA mismatch repair gene mutations. Eur. Urol 75, 378–382 (2019). [PubMed: 30337059]
58. Antonarakis ES, et al. CDK12-altered prostate cancer: clinical features and therapeutic outcomes to standard systemic therapies, poly (ADP-ribose) polymerase inhibitors, and PD-1 inhibitors. JCO Precis. Oncol 4, 370–381 (2020). [PubMed: 32462107]
59. Wu YM, et al. Inactivation of CDK12 delineates a distinct immunogenic class of advanced prostate cancer. Cell 173, 1770–1782 e1714 (2018). [PubMed: 29906450]

METHODS REFERENCES

60. Chen CD, et al. Molecular determinants of resistance to antiandrogen therapy. Nat. Med 10, 33–39 (2004). [PubMed: 14702632]
61. Wang L, et al. VSTM2A overexpression is a sensitive and specific biomarker for mucinous tubular and spindle cell carcinoma (MTSCC) of the kidney. Am. J. Surg. Pathol 42, 1571–1584 (2018). [PubMed: 30285995]
62. Bernard A, et al. Rph1/KDM4 mediates nutrient-limitation signaling that leads to the transcriptional induction of autophagy. Curr. Biol 25, 546–555 (2015). [PubMed: 25660547]
63. Martinez Molina D, et al. Monitoring drug target engagement in cells and tissues using the cellular thermal shift assay. Science 341, 84–87 (2013). [PubMed: 23828940]
64. Jafari R, et al. The cellular thermal shift assay for evaluating drug target interactions in cells. Nat. Protoc 9, 2100–2122 (2014). [PubMed: 25101824]
65. Palanisamy N, et al. The MD Anderson prostate cancer patient-derived xenograft series (MDA PCa PDX) captures the molecular landscape of prostate cancer and facilitates marker-driven therapy development. Clin. Cancer Res 26, 4933–4946 (2020). [PubMed: 32576626]
66. Yu JL, et al. Liver metastasis restrains immunotherapy efficacy via macrophage-mediated T cell elimination. Nat. Med 27, 152–164 (2021). [PubMed: 33398162]
67. Sanjana NE, Shalem O & Zhang F Improved vectors and genome-wide libraries for CRISPR screening. Nat. Methods 11, 783–784 (2014). [PubMed: 25075903]
68. Dobin A, et al. STAR: ultrafast universal RNA-seq aligner. Bioinformatics 29, 15–21 (2013). [PubMed: 23104886]
69. Love MI, Huber W & Anders S Moderated estimation of fold change and dispersion for RNA-seq data with DESeq2. Genome Biol 15, 550 (2014). [PubMed: 25516281]
70. Robinson MD, McCarthy DJ & Smyth GK edgeR: a Bioconductor package for differential expression analysis of digital gene expression data. Bioinformatics 26, 139–140 (2010). [PubMed: 19910308]
71. Afshinnia F, et al. Lipidomic signature of progression of chronic kidney disease in the chronic renal insufficiency cohort. Kidney Int. Rep 1, 256–268 (2016). [PubMed: 28451650]
72. Bligh EG & Dyer WJ A rapid method of total lipid extraction and purification. Can. J. Biochem. Physiol 37, 911–917 (1959). [PubMed: 13671378]
73. Cajka T & Fiehn O LC-MS-based lipidomics and automated identification of lipids using the LipidBlast in-silico MS/MS library. Methods Mol. Biol 1609, 149–170 (2017). [PubMed: 28660581]

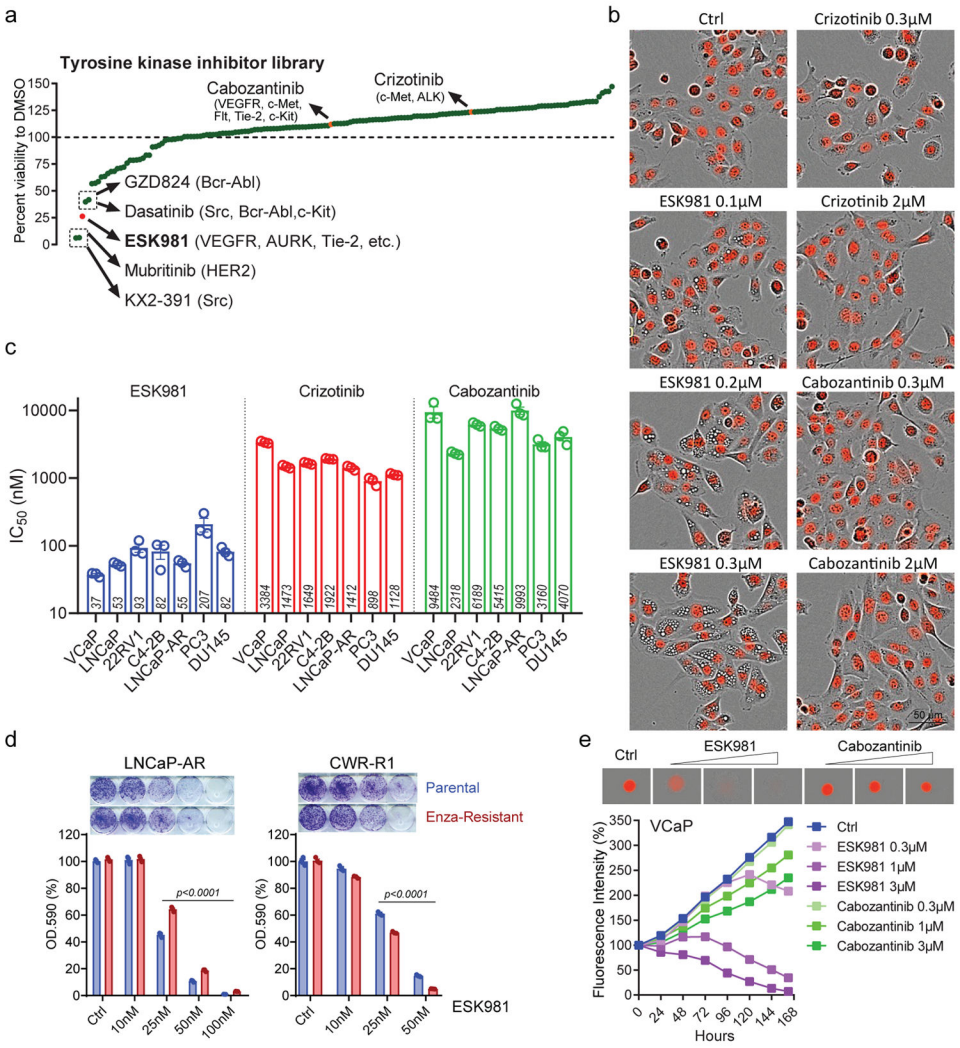

Fig. 1. ESK981 inhibits the growth of prostate cancer cells *in vitro* and is associated with a vacuolization morphology.

(a) The percentage viabilities of DU145 cells treated with ESK981 or 167 other tyrosine kinase inhibitors (all at 300 nM) when compared to a DMSO vehicle control in a long term survival assay. The top five most inhibitory compounds, as well as cabozantinib and crizotinib (highlighted in orange), and their respective targets are indicated. ESK981 is highlighted in red.

(b) Morphological differences of nuclear-restricted RFP-expressing DU145 cells treated with increasing concentrations of ESK981, crizotinib, or cabozantinib for 24 hours. Fluorescence and phase contrast images were taken by IncuCyte ZOOM from three independent experiments, with representative images shown.

(c) A long-term survival assay was used to calculate the half-maximum inhibitory concentration (IC_{50}) after two weeks of incubation with the serial dilutions of indicated drugs. IC_{50} of ESK981, crizotinib, and cabozantinib in a panel of prostate cancer cell lines are plotted as mean ± SEM from three independent experiments.

(d) ESK981 was effective against enzalutamide (Enza)-resistant cell lines. LNCaP-AR and CWR-R1 enzalutamide-resistant cells were maintained in 5 μM and 20 μM enzalutamide

medium, respectively, *in vitro*. Long-term survival (two weeks) was assayed by absorbance of crystal violet at OD.590. Data were analyzed by two-tailed unpaired t test from three independent experiments and presented as mean ± SEM. P-value indicated.

(e) VCaP-RFP cells were cultured for three days in ultralow attachment plates to form 3D tumor spheroids prior to the indicated drug treatments. Increasing concentrations of ESK981 and cabozantinib were added over the indicated time period. Fluorescence intensity of 3D spheroids was measured by IncuCyte ZOOM.

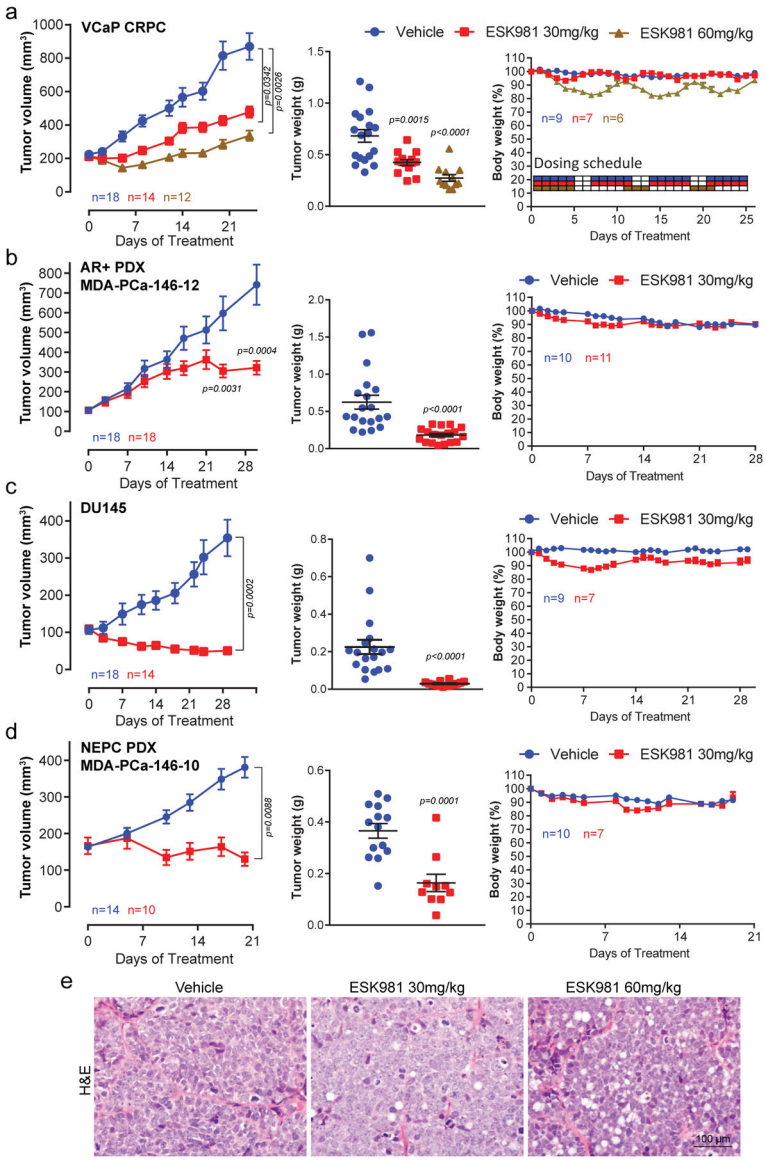

Fig. 2. ESK981 inhibits the growth of diverse preclinical models of prostate cancer *in vivo*.

(a) Castration-resistant VCaP tumors (VCaP CRPC) were established subcutaneously in castrated male SCID mice, and treated with vehicle, 30 mg/kg, or 60 mg/kg ESK981. Average tumor volumes were monitored twice per week, n=number of tumors (left). Individual VCaP CRPC tumor weights were measured at study endpoint, n=number of tumors (middle). Percent body weight changes and dosing schedule of VCaP CRPC model, n=number of mice (right). Data were analyzed by two-tailed unpaired t test and presented as mean ± SEM. N and P-value indicated.

(b) Androgen receptor $(AR)^+$ and ERG^+ prostate patient-derived xenograft (PDX) MDA-PCa-146-12 were established subcutaneously in non-castrated SCID mice and treated with vehicle or 30 mg/kg ESK981. Average tumor volumes were monitored twice per week, n=number of tumors (left). Tumor weights from individual tumors at study endpoint, n=number of tumors (middle). Percent body weight changes of MDA-PCa-146-12 tumor-

bearing mice, n=number of mice (right). Data were analyzed by two-tailed unpaired t test and presented as mean ± SEM. N and P-value indicated.

(c) DU145 tumors were established subcutaneously in non-castrated SCID mice and treated with vehicle or 30 mg/kg ESK981. Average tumor volumes were monitored twice per week, n=number of tumors (left). Individual tumor weights were measured at study endpoint, n=number of tumors (middle). Percent body weight changes of DU145 tumor-bearing mice, n=number of mice (right). Data were analyzed by two-tailed unpaired t test and presented as mean ± SEM. N and P-value indicated.

(d) Neuroendocrine (NEPC) prostate PDX MDA-PCa-146-10 were established in non-castrated SCID mice and treated with vehicle or 30 mg/kg ESK981. Tumor volumes were monitored twice per week, n=number of tumors (left). Individual tumor weights were measured at study endpoint, n=number of tumors (middle). Percent body weight changes of MDA-PCa-146-10 tumor-bearing mice, n=number of mice (right). Data were analyzed by two-tailed unpaired t test and presented as mean ± SEM. N and P-value indicated.

(e) Representative H&E images from three independent experiments showing a dose-dependent induction of a vacuolization morphology from VCaP CRPC tumors treated with vehicle, 30 mg/kg, or 60 mg/kg ESK981 for five days.

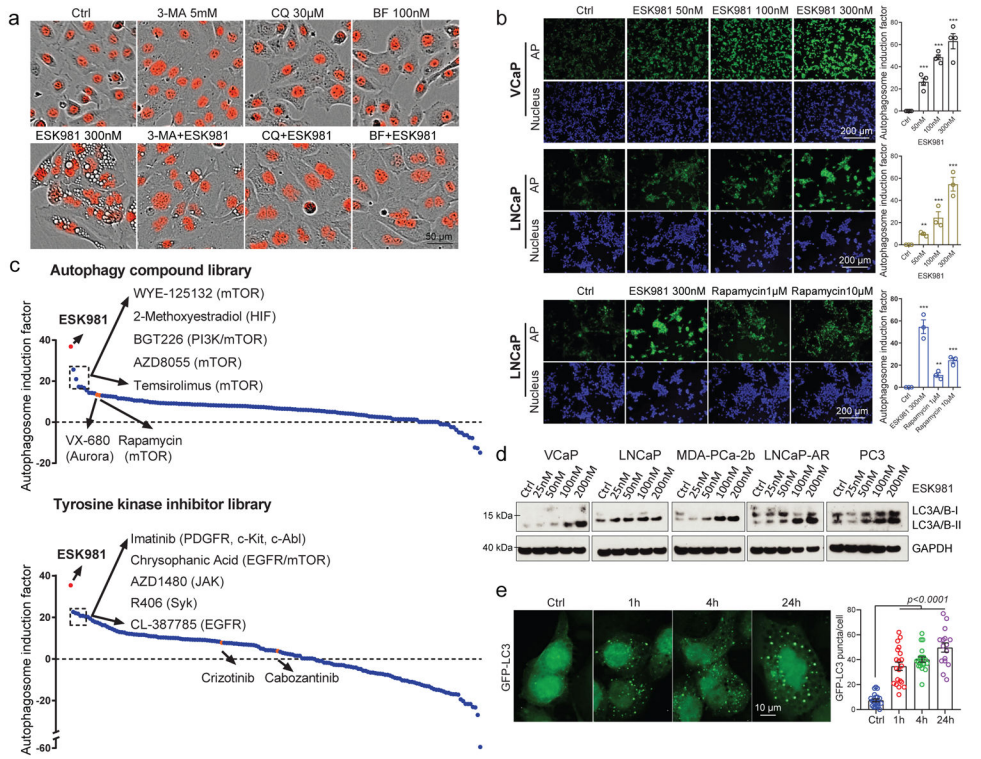

Fig. 3. ESK981 induces accumulation of autophagosomes in prostate cancer cells.

(a) Representative morphologies of DU145-RFP cells from three independent experiments treated with either ESK981, autophagy inhibitors (3-methyladenine [3-MA], chloroquine [CQ], bafilomycin A_1 [BF]), or a combination of ESK981 and one additional autophagy inhibitor for six hours. Red indicates nuclei.

(b) VCaP and LNCaP cells were treated with increasing concentrations of ESK981 for 24 hours. Autophagosome induction activity was measured with CYTO-ID®, and the quantification of autophagosomes are shown on the right. Rapamycin served as a positive control for autophagy induction. Data were analyzed by two-tailed unpaired t test from three (LNCaP) and four (VCaP) independent experiments and presented as mean ± SEM. **p<0.01; ***p<0.001.

(c) Autophagosome induction activity of ESK981 (in red), measured with CYTO-ID®, when compared to an autophagy-related compound library consisting of 154 compounds (top) or a tyrosine kinase inhibitor library consisting of 167 compounds (bottom). DU145 cells were treated with ESK981 or the other compounds (all at 300 nM) for 24 hours. The top five compounds and their respective targets are indicated. VX-680 and rapamycin are highlighted in orange in autophagy-related compound library. Crizotinib and cabozantinib are highlighted in orange in tyrosine kinase inhibitor library. Targets of highlighted compounds are indicated in parentheses.

(d) The indicated prostate cancer cell lines were treated with increasing concentrations of ESK981 for 24 hours. LC3 levels were assessed by western blot, with GAPDH serving as a loading control.

(e) Representative images of GFP-LC3 puncta in DU145 cells with 300 nM ESK981 treatment for various times. Quantifications of GFP-LC3 puncta from Ctrl (n=20 analyzed

cells), 1h (n=20 analyzed cells), 4h (n=20 analyzed cells), and 24h (n=16 analyzed cells) are shown on the right. Data were analyzed by two-tailed unpaired t test and presented as mean ± SEM. P-value indicated.

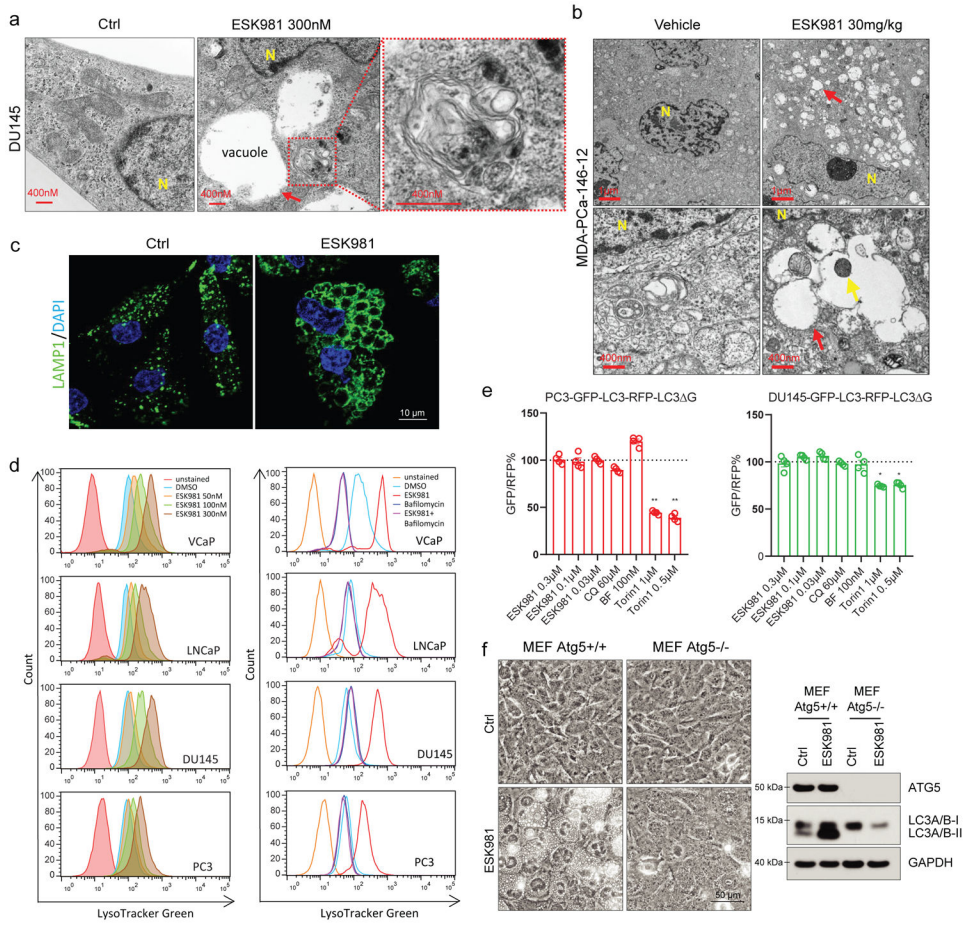

Fig. 4. ESK981 induces accumulation of lysosomes through inhibition of autophagic flux in prostate cancer cells.

(a) Representative TEM micrographs of DU145 cells after 300 nM ESK981 treatment for 24 hours from three independent experiments. Micrograph of ESK981-treated cell shows mostly clear vacuoles adjacent to an autophagic vacuole, which is magnified in the red dashed box. Red arrow indicates a mostly clear vacuole. N, nucleus.

(b) Representative micrographs of MDA-PCa-146-12 PDX tumors taken by TEM after five days of treatment from three independent experiments. Red arrows indicate vacuoles in ESK981 group, and yellow arrows indicate cellular materials inside the vacuole. N, nucleus.

(c) Representative immunofluorescence staining of LAMP1 in DU145 cells treated with control or 300 nM ESK981 for 24 hours from three independent experiments.

(d) Lysosomal activity was quantified by FACS after staining with LysoTracker Green. VCaP, LNCaP, PC3, and DU145 cells were treated with increasing concentrations of ESK981 for 24 hours (left). VCaP, LNCaP, PC3, and DU145 cells were treated with DMSO, ESK981 (300 nM), bafilomycin A_1 (100 nM), or ESK981-bafilomycin A_1 combination for 24 hours (right).

(e) Ratio of GFP/RFP signal in PC3 and DU145 GFP-LC3-RFP-LC3ΔG stable expressing cells with the indicated treatment for 24 hours. Data were analyzed by two-tailed unpaired t test from four independent experiments and presented as mean ± SEM. *p<0.05; **p<0.01.

(f) Paired MEF cells with either *Atg5* wild type ($Atg5^{+/+}$) or *Atg5* knockout ($Atg5^{-/-}$) were treated with 300 nM ESK981 for 24 hours. Representative morphologies are shown in phase contrast microscopy (left) from three independent experiments. ATG5 and LC3 protein levels were examined by western blot (right).

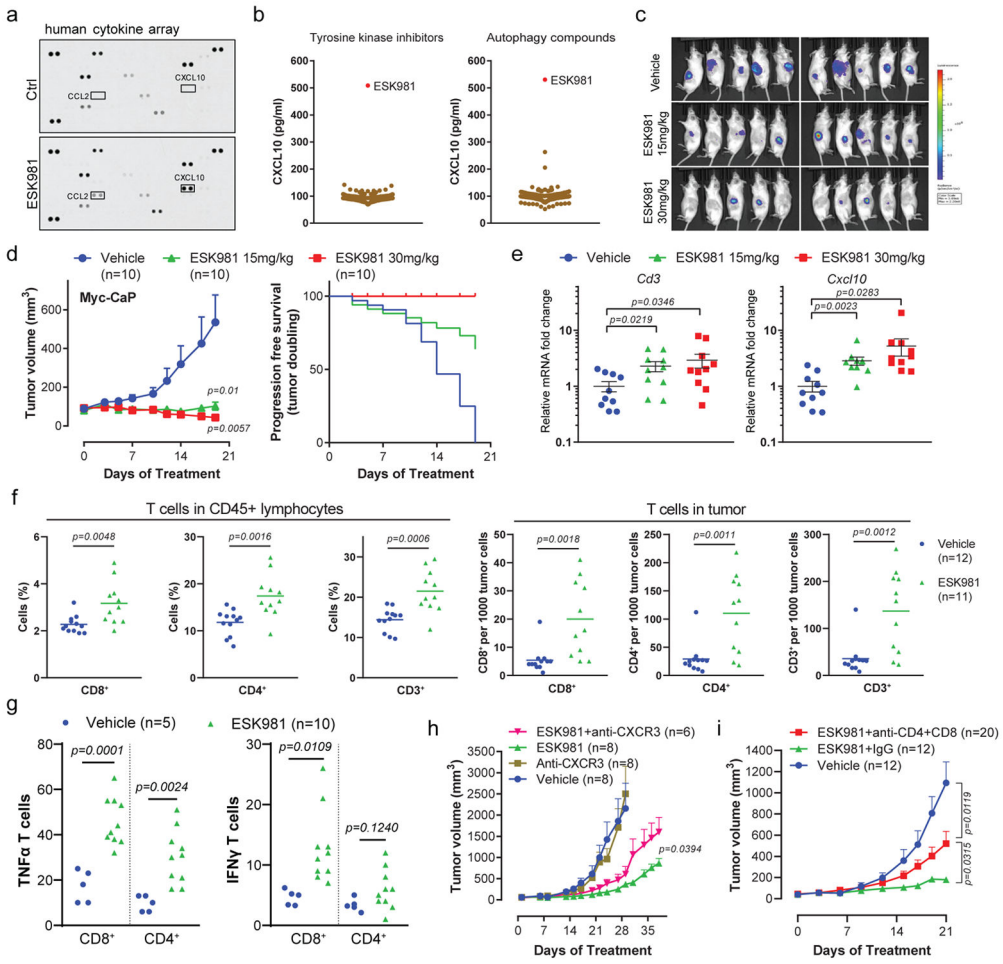

Fig. 5. ESK981 activates an anti-tumor immune response in immune-competent murine prostate cancer models.

(a) Human cytokine array using VCaP conditioned medium after 300 nM ESK981 treatment for 24 hours. CXCL10 and CCL2 are highlighted on the dot plots.

(b) CXCL10 ELISA using conditioned medium from VCaP cells treated with either ESK981 or two compound libraries (tyrosine kinase inhibitors and autophagy-related compounds), all at 300 nM for 24 hours. N=3 replicate wells per compound.

(c) Myc-CaP tumors were established in FVB mice and treated with vehicle or the indicated dose of ESK981. Bioluminescent imaging was performed on individual tumors at day 19. N=10 tumors per group.

(d) Average Myc-CaP tumor volumes from indicated treatment groups (left). Progression-free survival (tumor doubling) was calculated from individual tumors (right). Data were analyzed by two-tailed unpaired t test and presented as mean ± SEM. N=10 tumors per group, and P-values are indicated.

(e) *Cd3* and *Cxcl10* mRNA levels of individual Myc-CaP tumors treated with vehicle, 15 mg/kg, or 30 mg/kg ESK981. Data were analyzed by two-tailed unpaired t test and presented as mean ± SEM. N=10 tumors per group, and P-values are indicated.

(f) Flow cytometry quantification of $CD8^+$, $CD4^+$, and $CD3^+$ T cells in $CD45^+$ lymphocytes (left) and infiltrating Myc-CaP tumors (right) treated with vehicle or 15 mg/kg ESK981.

Data were analyzed by two-tailed unpaired t test and presented as mean and individual data points. N=number of tumors, and P-values are indicated.

(g) Flow cytometry quantification of TNFα or IFNγ-expressing $CD8^+$ and $CD4^+$ T cells infiltrating Myc-CaP tumors treated with vehicle or 15 mg/kg ESK981. Data were analyzed by two-tailed unpaired t test and presented as individual data points. N=number of tumors, and P-values are indicated.

(h) Average Myc-CaP tumor volumes from indicated treatment groups in FVB mice. Data are presented as mean ± SEM and p-values were analyzed by two-tailed unpaired t test at endpoint for ESK981 and ESK981+anti-CXCR3 groups. N=number of tumors, and P-value is indicated.

(i) Average Myc-CaP tumor volumes from indicated treatment groups in FVB mice. Data were analyzed by two-tailed unpaired t test and presented as mean ± SEM. N=number of tumors, and P-values are indicated.

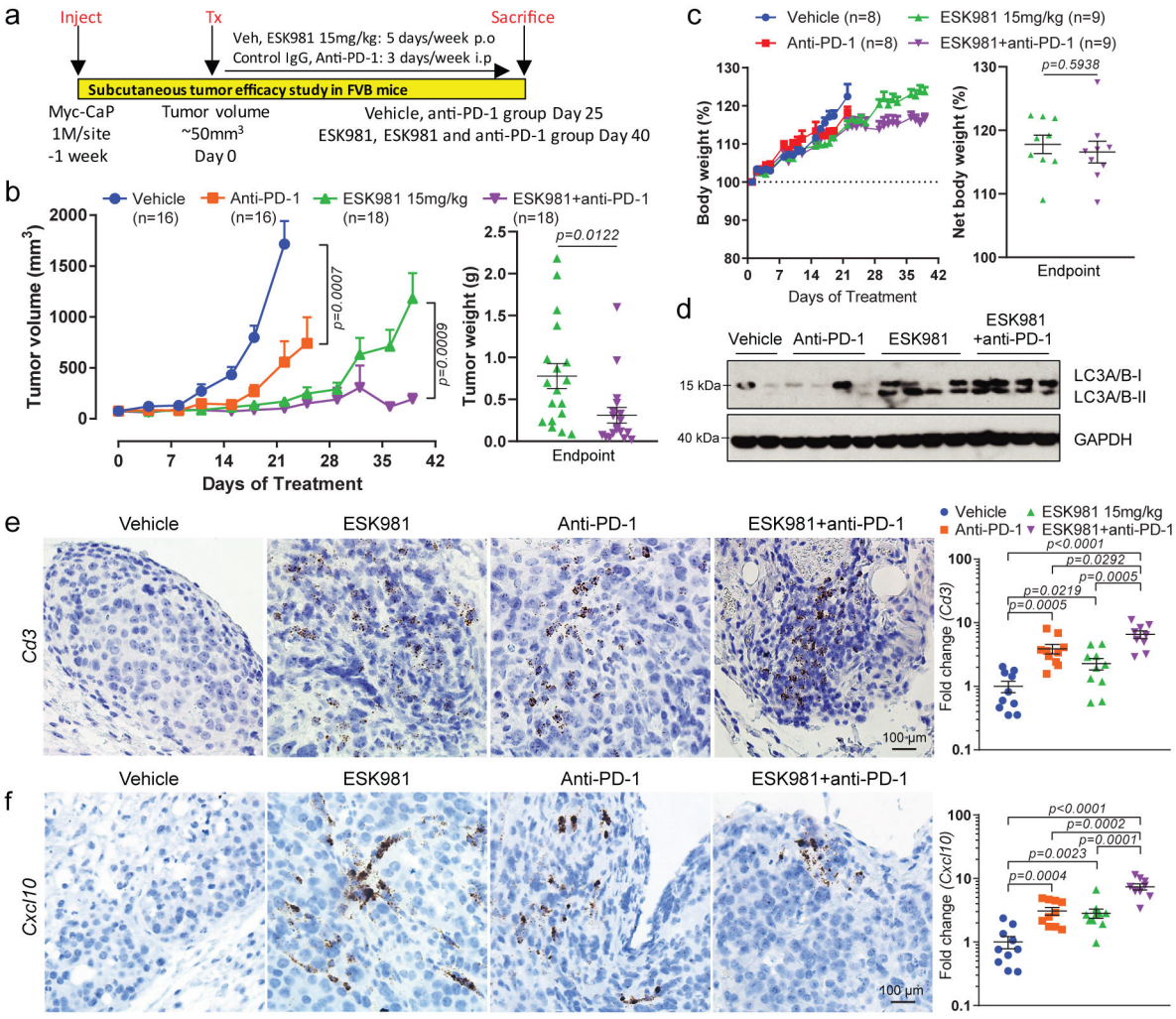

Fig. 6. ESK981 potentiates the effect of anti-PD-1 immunotherapy in immune-competent murine prostate cancer models.

(a) Illustration of Myc-CaP experimental design in immune-competent FVB mice. p.o, oral gavage. i.p, intraperitoneal.

(b) Average Myc-CaP tumor volumes from indicated treatment (left). Myc-CaP tumor weights were measured at endpoint from ESK981 and ESK981 plus anti-PD-1 (right). Data were analyzed by two-tailed unpaired t test and presented as mean ± SEM. N=number of tumors, and P-values are indicated.

(c) Percent body weight changes of Myc-CaP tumor-bearing mice receiving indicated treatment (left); data were presented as mean ± SEM. Net body weight changes were calculated by exclusion of tumor weight from total body weight in ESK981 and ESK981+anti-PD-1 treated mice at day 40 (right); data were analyzed by two-tailed unpaired t test and presented as mean ± SEM. N=number of mice, and P-value is indicated.

(d) Protein levels of LC3 from representative individual tumors measured by western blot after five days of the indicated treatment in Myc-CaP tumors. N=2 for vehicle; n=4 for anti-PD-1; n=4 for ESK981; n=4 for ESK981+anti-PD-1 with three independent experiments.

(e) Representative *Cd3* RNA ISH from the indicated Myc-CaP tumors with three independent experiments (left). For a complementary method of assessing *Cd3* levels, *Cd3* mRNA levels were quantified by qPCR in individual tumors treated with vehicle (n=10 tumors), ESK981 15 mg/kg (n=10 tumors), anti-PD-1 (n=10 tumors), ESK981 and anti-PD-1 (n=9 tumors) (right). Data from vehicle and ESK981 15 mg/kg tumors were included for different comparison purposes in Fig. 5e. Data were analyzed by two-tailed unpaired t test and presented as mean ± SEM. P-value indicated.

(f) Representative *Cxcl10* RNA ISH from the indicated Myc-CaP tumors with three independent experiments (left). For a complementary method of assessing *Cxcl10* levels, *Cxcl10* mRNA levels were quantified by qPCR in individual tumors treated with vehicle (n=10 tumors), ESK981 15 mg/kg (n=10 tumors), anti-PD-1 (n=10 tumors), ESK981 and anti-PD-1 (n=9 tumors), after three weeks of the indicated treatments in Myc-CaP tumors (right). Data from vehicle and ESK981 15 mg/kg tumors were included for different comparison purposes in Fig. 5e. Data were analyzed by two-tailed unpaired t test and presented as mean ± SEM. P-value indicated.

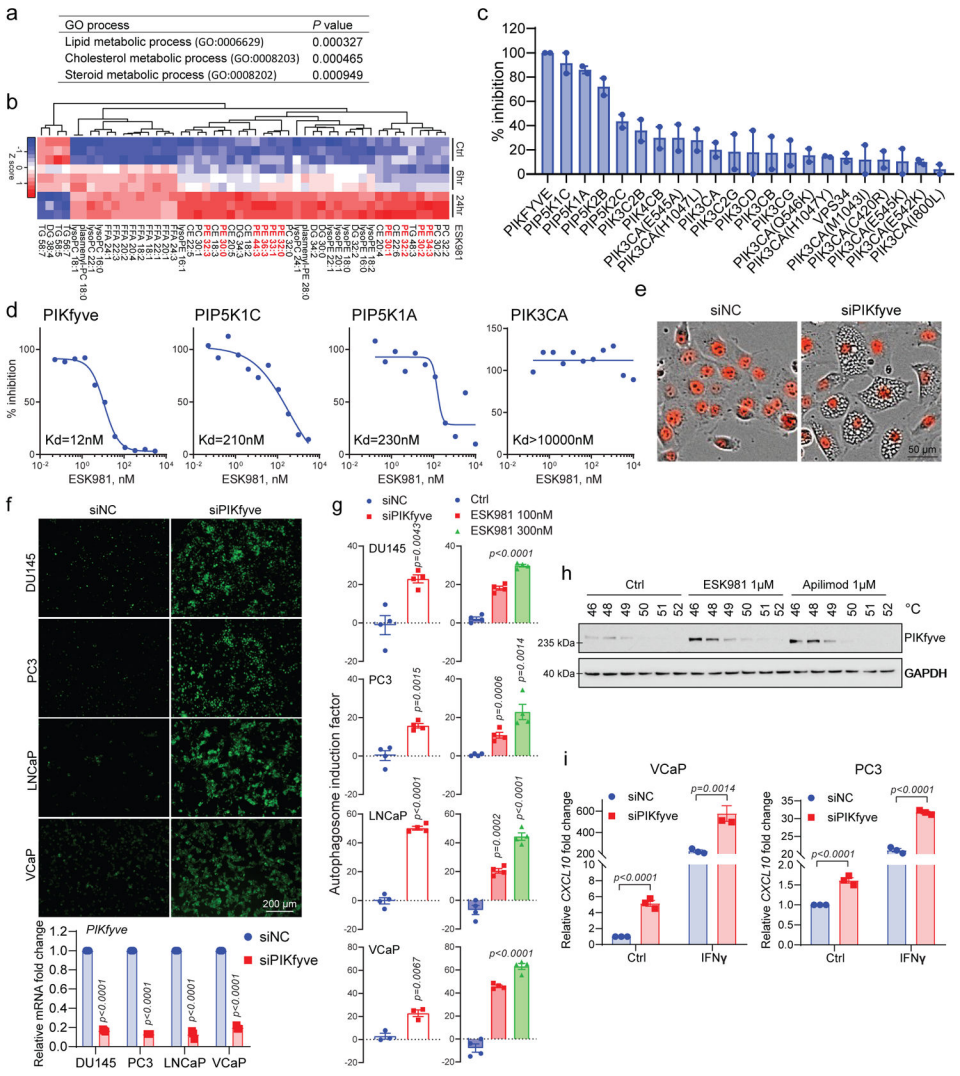

Fig. 7. Identification of lipid kinase PIKfyve as the target of ESK981-induced effects on autophagy and CXCL10 levels.

(a) Gene ontology analysis for top elevated genes after 300 nM ESK981 in VCaP cells for 6 and 24 hour treatments. The top three processes are listed.

(b) Heatmap representation of untargeted lipidomics analysis after 300 nM ESK981 treatment for 6 and 24 hours in VCaP cells. N=3 technical replicates per group. The PE class is highlighted in red.

(c) Percent inhibition of 1 μM ESK981 against a panel of 22 lipid kinases. Data are presented as mean with individual data points.

(d) Representative dissociation constant (Kd) curve of ESK981 against lipid kinases PIKfyve, PIP5K1C, PIP5K1A, and PIK3CA.

(e) Representative morphology of DU145-RFP cells with control siRNA or *PIKFYVE* siRNA with three independent experiments.

(f) Fluorescent images showing autophagosome levels measured with CYTO-ID® assay in DU145, PC3, LNCaP, and VCaP after siRNA knockdown of *PIKFYVE* (top). *PIKFYVE* mRNA levels were quantified by qPCR in indicated cells after siNC or si*PIKFYVE*

knockdown (bottom). Data were analyzed by two-tailed unpaired t test from three independent experiments and presented as mean ± SEM. P-value indicated.
(g) Quantification of autophagosome induction activity measured with CYTO-ID® assay in DU145, PC3, LNCaP, and VCaP after siRNA knockdown of *PIKFYVE* or treatment with ESK981. Data were analyzed by two-tailed unpaired t test from three independent experiments for VCaP siRNA and four independent experiments for the remaining conditions. Data are presented as mean ± SEM. P-values indicated.
(h) Cellular thermal shift assay (CESTA) of VCaP cells treated with control, 1 μM ESK981, or 1 μM apilimod for 2 hours with three independent experiments.
(i) *CXCL10* mRNA levels in VCaP or PC3 cells after siRNA knockdown of a non-targeting control (siNC) or *PIKFYVE* (si*PIKFYVE*) with the indicated treatment for 24 hours. Data were analyzed by two-tailed unpaired t test from three independent experiments and presented as mean ± SEM. P-value indicated.

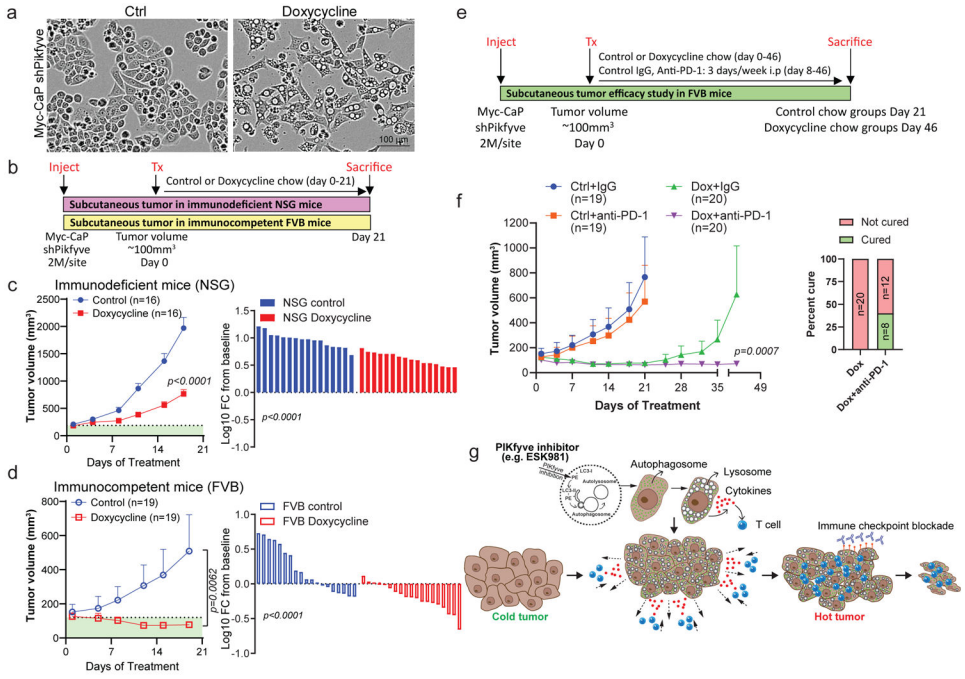

Fig. 8. Genetic inhibition of *Pikfyve* potentiates the therapeutic benefit of anti-PD-1 immunotherapy in immune-competent murine models.

(a) Representative images of doxycycline inducible sh*Pikfyve* Myc-CaP cells with or without 1 μg/ml doxycycline treatment for 72 hours from three independent experiments.

(b) Schematic illustration of sh*Pikfyve* Myc-CaP experimental design in immunodeficient mice (NSG) and immunocompetent mice (FVB).

(c) Average tumor volume of sh*Pikfyve* Myc-CaP with or without doxycycline chow in NSG mice (left). Percent changes in sh*Pikfyve* Myc-CaP tumor volume represented by waterfall plot in NSG mice (right). Data were analyzed by two-tailed unpaired t test and presented as mean ± SEM. N=number of tumors and P-value is indicated.

(d) Average tumor volume of sh*Pikfyve* Myc-CaP with or without doxycycline chow in FVB mice (left). Percent changes in sh*Pikfyve* Myc-CaP tumor volume represented by waterfall plot in FVB mice (right). Data were analyzed by two-tailed unpaired t test and presented as mean ± SEM. N=number of tumors and P-value is indicated.

(e) Schematic illustration of sh*Pikfyve* Myc-CaP experimental design in immunocompetent mice. i.p, intraperitoneal.

(f) Average tumor volume of sh*Pikfyve* Myc-CaP with control chow or doxycycline chow and/or mouse control IgG or anti-PD-1 antibody for 6 weeks (left). Data from control chow or doxycycline chow groups were included in Fig. 8d for different comparison purposes. Percentage cure rate defined as ratio of complete tumor regression on groups of doxycycline chow and/or mouse anti-PD-1 antibody (right). Data were analyzed by Mann-Whitney test and presented as mean ± SEM. N=number of tumors and P-value is indicated.

(g) Model of ESK981's mechanism of action and its anti-tumor activity, described in the main text.